Zeitschrift: IABSE reports = Rapports AIPC = IVBH Berichte

Band: 79 (1998)

Rubrik: Working session: Assessment by analysis and experiment. Papers and posters

Working Session

Assessment by Analysis and Experiment

Papers and Poster

Leere Seite
Blank page
Page vide

Three-Dimensional Response Spectrum Analysis for Multicomponent Seismic Excitation

Ioannis E. AVRAMIDIS
Prof.
Aristotle Univ. of Thessaloniki
Thessaloniki, Greece

Kyriakos ANASTASSIADIS
Prof.
Aristotle Univ. of Thessaloniki
Thessaloniki, Greece

Summary

Within the framework of response spectrum analysis, a general solution for the three-component orthotropic seismic excitation problem is presented. The contributions from three different orthogonal earthquake components are combined in a rational manner to the maximum and minimum values of any structure response quantity. The critical orientation of the seismic input associated with these values is also determined. The method incorporates in its formulation the Penzien-Watabe model of ground motion. Therefore, in contrast to the SRSS rule, it can explicitly account for the correlation of the three seismic components, which makes it particularly usefull in the dynamic analysis of curved bridges. All given relations are easy to implement in current standard dynamic analysis software.

1. Introduction

According to the model of Penzien and Watabe [1], the three translational seismic motion components on a specific point of the ground are statistically uncorrelated along a well-defined orthogonal system of axes whose orientation remains reasonably stable over time during the strong motion phase of an earthquake. This system of principal axes of the ground motion is oriented such that the major principal axis "p" is horizontal and directed towards the epicenter, the intermediate principal axis "w" is in the transverse (orthogonal) direction, and the minor principal axis "v" is vertical (The choosen notation shall remind of Penzien-Watabe model). This orthotropic ground motion is described by three generally independent response spectra S^a, S^b and S^c, with $S^a>S^b>S^c$.

In the special case of equal horizontal components $S^a=S^b$, the extreme values of the structure's response quantities do not depend on the direction "a" of the epicentral seismic component [2,3]. However, in the general case of $S^a>S^b$, the extreme value of a response quantity strongly depends on this direction. Therefore, the determination of the most unfavorable (critical) epicentral direction for each response quantity is of great practical interest. Smeby and Der Kiureghian [4] determined the critical direction in case of analogous response spectra $S^a=\gamma S^b$, where $0<=\gamma<=1$. Also, Anastassiadis [3] and Lopez and Torres [5] determined the critical direction for the more general case of arbitrary response spectra.

In this paper, on the basis of the Penzien-Watabe idealization, the tensorial properties of the extreme values of response are presented. The critical epicentral direction as well as the correspondent maximum and minimum values of an arbitrary response quantity can be straightforwardly deduced from these properties.

2. Notation

A fixed global orthogonal reference system Oxyz is used for the structure. The spectra S^a or S^b are applied individually in the direction of the x- or y-axis according to Figure 1. The corresponding peak probable values of a typical response quantity R (force or displacement) are symbolized as $R_{,xa}$, $R_{,xb}$, $R_{,ya}$ and $R_{,yb}$ (Figure 1a,b,c,d), where the first subscript refers to motion in direction x or y and the second (a or b) to the input earthquake spectrum (S^a or S^b). $R_{,x}$ and $R_{,y}$ symbolize the extreme values of a typical response quantity R produced from a bidirectional excitation with epicentral direction along the axis x or y respectively (Figure 1e,f). An analogous notation is used for the variable system of principal axes Opwv.

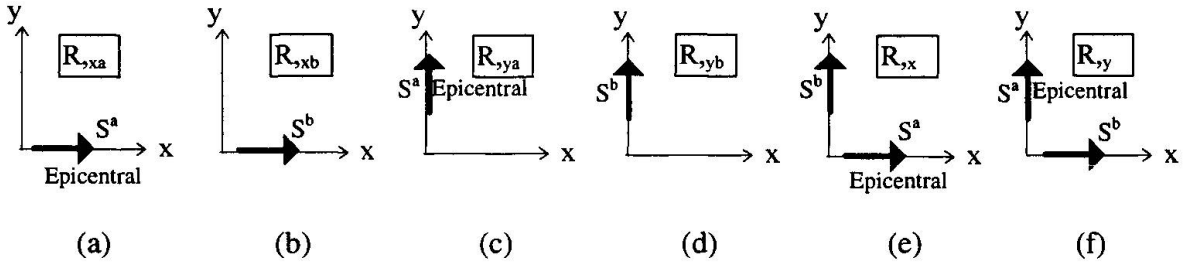

Figure 1. Response parameter notation

3. Tensorial properties - Critical direction

We assume that the epicentral principal axis p of the ground motion is defined in terms of an angle θ relative to the x axis of the fixed reference system of the structure (Figure 2). If S^a is the design spectrum in the direction of p axis and S^b the design spectrum in the direction of w axis, the probable extreme value of a response quantity R is [6] :

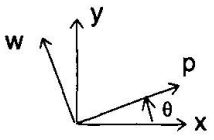

Figure 2. Definition of angle θ

$$R_{,p}^2 = R_{,pa}^2 + R_{,wb}^2 = \sum_i \sum_j \varepsilon_{i,j} \left(R_{i,pa} R_{j,pa} + R_{i,wb} R_{j,wb} \right) \qquad (1a)$$

In the above expression, $\varepsilon_{i,j}$ denotes the correlation coefficient between the responses in modes i and j, and $R_{i,pa}$ and $R_{i,wb}$ denote the modal values of quantity R for the excitations defined by the indices after comma. If S^b is the design spectrum in the direction of p axis and S^a the design spectrum in the direction of w axis, we obtain the probable extreme value

$$R_{,w}^2 = R_{,pb}^2 + R_{,wa}^2 = \sum_i \sum_j \varepsilon_{i,j} \left(R_{i,pb} R_{j,pb} + R_{i,wa} R_{j,wa} \right) \qquad (1b)$$

and the correlation term

$$R_{pw} = R_{pw,a} - R_{pw,b} = \sum_i \sum_j \varepsilon_{i,j} \; (R_{i,pa} R_{j,wa} - R_{i,pb} R_{j,wb}) \qquad (1c)$$

The modal values $R_{i,p}$ and $R_{i,w}$ are connected to the modal values $R_{i,x}$ and $R_{i,y}$ through the following relations, which are independent of the used earthquake spectrum S^a or S^b :

$$R_{i,p} = + R_{i,x} \cos\theta + R_{i,y} \sin\theta \qquad (2a)$$

$$R_{i,w} = - R_{i,x} \sin\theta + R_{i,y} \cos\theta \qquad (2b)$$

Inserting these relations in the right-hand terms of (1) we obtain

$$R_{,p}^2 = R_{,x}^2 \cos^2\theta + R_{,y}^2 \sin^2\theta + R_{xy} \sin 2\theta \qquad (3a)$$

$$R_{,w}^2 = R_{,x}^2 \sin^2\theta + R_{,y}^2 \cos^2\theta - R_{xy} \sin 2\theta \qquad (3b)$$

$$R_{pw} = - (\tfrac{1}{2}) (R_{,x}^2 - R_{,y}^2) \sin 2\theta + R_{xy} \cos 2\theta \quad , \qquad (3c)$$

where

$$R_{,x}^2 = R_{,xa}^2 + R_{,yb}^2 = \sum_i \sum_j \varepsilon_{i,j} \; (R_{i,xa} R_{j,xa} + R_{i,yb} R_{j,yb}) \qquad (4a)$$

$$R_{,y}^2 = R_{,xb}^2 + R_{,ya}^2 = \sum_i \sum_j \varepsilon_{i,j} \; (R_{i,xb} R_{j,xb} + R_{i,ya} R_{j,ya}) \qquad (4b)$$

$$R_{xy} = R_{xy,a} - R_{xy,b} = \sum_i \sum_j \varepsilon_{i,j} \; (R_{i,xa} R_{j,ya} - R_{i,xb} R_{j,yb}) \qquad (4c)$$

It is important to note that relations (3) are similar to the transformation rules for the components of a symmetric second order tensor. Consequently, the four quantities $R_{,x}^2$, $R_{,y}^2$ and $R_{xy} = R_{yx}$ can be considered as components of a symmetric second order tensor, expressed analytically by matrices

$$\begin{bmatrix} R_{,x}^2 & R_{xy} \\ R_{yx} & R_{,y}^2 \end{bmatrix} \qquad \text{and} \qquad \begin{bmatrix} R_{,p}^2 & R_{pw} \\ R_{wp} & R_{,w}^2 \end{bmatrix}$$

in the Oxy and Opw reference system respectively. Due to its tensorial character, the arbitrary response quantity R is characterized by the following properties which are common to all symmetric second order tensors :

(a) The trace and the determinant of the above matrices are not dependent on the orientation of the earthquake excitation :

$$R_{,x}^2 + R_{,y}^2 = R_{,p}^2 + R_{,w}^2 \quad \text{and} \quad R_{,x}^2 R_{,y}^2 - R_{xy}^2 = R_{,p}^2 R_{,w}^2 - R_{pw}^2$$

(b) There is a specific earthquake orientation defined by the axes (I, II) for which the correlation term R_{pw} vanishes. This specific orientation is determined by the critical angle (see eq. 3c) :

$$\theta_{cr} = (1/2) \tan^{-1}(2R_{xy}/(R_{,x}^2 - R_{,y}^2)) \quad (5)$$

The corresponding response quantity R takes the following maximum and minimum values :

$$\max R^2 = R_{,I}^2 = (R_{,x}^2 + R_{,y}^2)/2 + \sqrt{[(R_{,x}^2 - R_{,y}^2)/2]^2 + R_{xy}^2} \quad (6a)$$

$$\min R^2 = R_{,II}^2 = (R_{,x}^2 + R_{,y}^2)/2 - \sqrt{[(R_{,x}^2 - R_{,y}^2)/2]^2 + R_{xy}^2} \quad (6b)$$

(c) The correlation term R_{pw} takes its maximum value

$$\max R_{pw} = R_{12} = (1/2)(R_{,I}^2 - R_{,II}^2)$$

for a seismic excitation along axes (1,2) defined by the angle bisecting the axes (I, II). For these seismic directions, a response quantity R takes the value

$$R_{,1}^2 = R_{,2}^2 = (1/2)(R_{,I}^2 + R_{,II}^2)$$

i.e., the interchange of the input design spectra S^a and S^b along the axes 1 and 2 does not affect the peak value of R.

It is clear from the preceding considerations that the calculation of the maximum and minimum values of an arbitrary response quantity requires four independent dynamic analyses of the structure, applying input spectra S^a and S^b as shown in Figures 1a to 1d. All necessary terms, e.g., the modal values in the right-hand sides of equations (4), are routinely calculated by current standard linear dynamic analysis programs. Then, using (4), $R_{,x}^2$, $R_{,y}^2$ and R_{xy} can be computed, and from (6a,b) the maximum and minimum values of any response quantity R can be immediately obtained, with no need to previously calculating the critical angle θ. Finally, the contribution of the vertical seismic component is to be added to the above values, according the SRSS combination rule. It is obvious that all mentioned relations can be easily implemented in current standard software for multicomponent seismic analysis.

4. Conclusions

A general solution for the three-component orthotropic seismic excitation problem is presented. It offers, within the framework of response spectrum analysis, a rational procedure for determining the maximum and minimum values of any given response quantity R of a structure. It also provides a simple means of determining the critical orientation θ associated with the extreme values of R. In contrast to the SRSS rule prescribed by many design codes, the presented method can explicitly account for the correlation of the different seismic components by incorporating in its formulation the Penzien-Watabe model of ground motion. This fact makes it particularly usefull in the dynamic analysis of curved bridges. All necessary relations are of a computationally simple form and can be easily implemented in current standard dynamic analysis software.

References

[1] Penzien, J. and Watabe, M., Characteristics of 3-D Earthquake Ground Motions, Earthquake Engineering and Structural Dynamics, 1975, 3, 365-373.

[2] Anastassiadis, K. and Avramidis, I.E., Unfavourable directions of seismic excitation for multistorey buildings (in greek), in Proc. of the 1st Greek Conf. on Earthq. Eng. and Eng. Seismology, 252-263, March 1992, Athens.

[3] Anastassiadis, K., Directions sismiques défavorables et combinaisons défavorables des efforts, Annales de l' I.T.B.T.P., 1993, no.512, 83-97.

[4] Smeby, W. And Der Kiuregian, A., Modal combination rules for multicomponent earthquake excitation, Earthquake Engineering and Structural Dynamics, 1985, 13, 1-12.

[5] Lopez, O.A. and Torres, R., Determination of maximum structural response to two horizontal motion components applied along any arbitrary directions for application to building codes, XI World Conference Earthquake Engineering, Acapulco, paper No. 619, Mexico, June 1996.

[6] Der Kiureghian, A., A response spectrum method for random vibration analysis of MDF systems, Earthquake Engineering and Structural Dynamics, 1985, 9, 419-435.

Leere Seite
Blank page
Page vide

Small Strain Non-Linear Relations for 3D Space Beam Systems

Milan VASEK
Assoc. Prof.
Czech Techn. Univ.
Praha, Czech Republic

Milan Vasek, born 1941, received his civil eng. degree from the Czech Techn. Univ. Prague and PhD in 1974. He is currently teaching at the Czech Techn. Univ. and working as consulting and forensic eng. He was as visiting Prof. at Mie Univ. in Japan 1991 and Fulbright scholar at Pittsburgh Univ. in USA in 1995.

Summary

This contribution is dedicated to the improvement of the geometric non-linear solution of 3D beam space structural system based on a finite element approach. The improved relations are based on all terms of the energy expression for the axial deformation. The energy due to the deformation caused by St.Venant torsion of 3D-beam element is taken into the account for the geometric non-linear behavior of the 3D element. The influence of each component of a joint deflection on the others within the non-linear solution of the element is clearly separated. The effect of the elastically constrained members is included in relations. The new cross sectional properties of the 3D beam are presented.

1. Introduction

Geometric non-linear behavior of space structures is investigated by many researchers. The classical approach is dealing with the geometric stiffness matrix $\mathbf{k}_G$. The nodal forces are given by the well known equation (1) from [1].

$$\mathbf{S} = (\mathbf{k}_E + \mathbf{k}_G) \mathbf{U} \qquad (1)$$

where **S** is the vector of nodal forces of the element, **U** is the vector of the nodal displacements, $\mathbf{k}_E$ is the elastic stiffness matrix and $\mathbf{k}_G$ is the geometric stiffness matrix.

The point of interest on the influence of semirigid connections together with the non-linear behavior of structure is described in [2], [3], [4], [5], [6]. Space structural frameworks are intensively used since 1980's. Papers dealing with these problems are published in proceedings on Space structures [4], [5]. At the work [9] are derived relations for the semirigid connections with respect to the all twelve degrees of freedom in the space. The solution which is based on the equation (1) is omitting higher order terms of the beam energy due to axial deformation. The concept of a geometric stiffness matrix is based on the simplification that the load imposed onto the structure is unchanged, during the load step increment. The relations which are introduced in this paper are not using any simplification and all the terms in the energy expression are used. As result of the approach leads to a clearly separated relations for each component of the deflection. The other effect of the approach is that the relations are more accurate then the previous equation (1). The detail derivation and the solution procedure is described in [6], [7], [8]. It is also

possible to introduce the effect of the semirigid connections as were derived by Toader at [9]. The derived results are corresponding to the relations for the plane frame structures in [10].

2. Non linear relations

2. 1 Basic Assumptions

The derivation is based on the following assumptions:
1) 3D members are straight without any imperfections
2) The local coordinate system of the member follows the right hand rule and is coincident with major principal axis of the member
3) Navier's hypothesis is valid for the cross-section of the member.
4) Torsion is assumed to be Saint Venant type, i. g. warping is neglected.
5) The load step increment is finite
6) The loads are acting on joints
7) The structural material is elastic-perfectly plastic
8) Local stability effects do not occur

2.2. The basic relations of geometric non-linear behavior

The relation between the nodal displacements and element deformations is described by

$$\mathbf{u}\,(x, y, z) = \mathbf{a}\ \mathbf{U}\,(u_1,u_2,u_3,.....u_n) \qquad (2)$$

where **u** is the vector of the element deformations and **U** is the vector of nodal displacements. Matrix **a** is the matrix of functions describing the geometrical relations between these displacements. Non-dimensional coordinates are introduced as $\xi = \frac{x}{L}, \zeta = \frac{y}{L}, \eta = \frac{z}{L}$, where x, y, z are dimensions in local coordinate system and L is the length of the 3D element (Fig.1)
The deformed length of an infinitesimally small element (Fig.2) can be expressed as

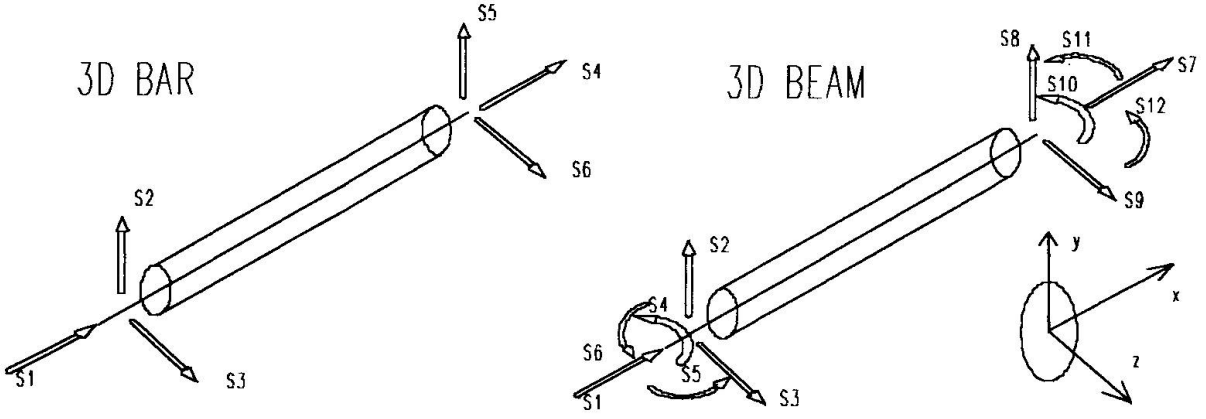

Fig.1: The 3D bar and beam member

$(1+\varepsilon_x^a)dx$ where the ε_x^a is the engineering axial strain and dx is the elements length. Applying Pythagora's theorem, the elongation of the element may be expressed as

$$[(1 + \varepsilon_x)dx]^2 = \left(dx + \frac{\partial u}{\partial x}dx\right)^2 + \left(\frac{\partial v}{\partial x}dx\right)^2 + \left(\frac{\partial w}{\partial x}dx\right)^2 \quad (3)$$

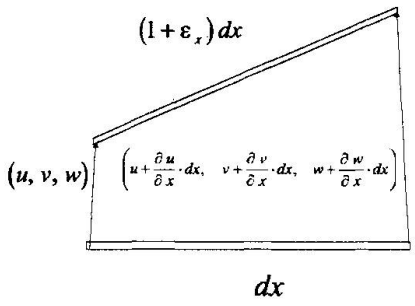

This can be simplified as:

$$\varepsilon_x\left(1 + \frac{\varepsilon_x}{2}\right) = \frac{\partial u}{\partial x} + \frac{1}{2}\left(\frac{\partial u}{\partial x}\right)^2 + \frac{1}{2}\left(\frac{\partial v}{\partial x}\right)^2 + \frac{1}{2}\left(\frac{\partial w}{\partial x}\right)^2 \quad (4)$$

The right hand side of equation (4) represents the component of the Green strain tensor e_{xx}. For the condition of small strain, we can write $(\varepsilon_x^a)^2 = 0$ and the Green tensor coincides with the engineering strain ε_x. If we introduce terms for the axial deformation due to bending to the expression (4) we receive

Fig.2: The beam element

$$\varepsilon_x = \frac{\partial u}{\partial x} + \frac{1}{2}\left(\frac{\partial v}{\partial x}\right)^2 + \frac{1}{2}\left(\frac{\partial w}{\partial x}\right)^2 - y\frac{\partial^2 u_y}{\partial x^2} - z\frac{\partial^2 u_z}{\partial x^2} \quad (5)$$

The energy of the member due to the axial deformation (5) can be expressed by equation (6)

$$U = \tfrac{1}{2}E\int_V \varepsilon^2 dV \quad (6)$$

The whole axial energy expression is expressed as:

$$U = \frac{E}{2}\int_0^L \oint_A \left\{\left(\frac{\partial u_x}{\partial x}\right)^2 + \left(\frac{\partial^2 u_y}{\partial x^2}\right)^2 y^2 + \left(\frac{\partial^2 u_z}{\partial x^2}\right)^2 z^2 + \frac{1}{4}\left(\frac{\partial u_x}{\partial x}\right)^4 + \frac{1}{4}\left(\frac{\partial u_z}{\partial x}\right)^4 + \frac{\partial u_x}{\partial x}\left(\frac{\partial^2 u_y}{\partial x^2}\right)^2 + \frac{\partial u_x}{\partial x}\left(\frac{\partial^2 u_z}{\partial x^2}\right)^2 \right. \quad (7)$$

$$-2\frac{\partial u_x}{\partial x}\frac{\partial^2 u_y}{\partial x^2}y - 2\frac{\partial u_x}{\partial x}\frac{\partial^2 u_{zy}}{\partial x^2}z + \frac{1}{2}\left(\frac{\partial u_y}{\partial x}\right)^2 - \left(\frac{\partial u_y}{\partial x}\right)^2\left(\frac{\partial^2 u_y}{\partial x^2}\right)y - \left(\frac{\partial u_y}{\partial x}\right)^2\left(\frac{\partial^2 u_z}{\partial x^2}\right)z - \frac{\partial^2 u_y}{\partial x^2}\left(\frac{\partial u_z}{\partial x}\right)^2 y$$

$$\left. -\left(\frac{\partial u_z}{\partial x}\right)^2\left(\frac{\partial^2 u_z}{\partial x^2}\right)z + \frac{\partial^2 u_y}{\partial x^2}y\frac{\partial^2 u_z}{\partial x^2}z \right\} dA\,dx$$

Let's express the deflection vector **u** in the form of nodal displacements using the equation (2) and perform the integration of the equation (7). After that, Castigliano's theorem (part 1) can be applied to the expression (7) with respect to the deflections u_1, u_2, ... u_{12},. We obtain the relations for the nodal forces S_1 , S_2 , ... S_6 for the 3D bar and S_1 , S_2 , ... S_{12} for the 3D beam. To express results in the matrix form we have to introduce new cross sectional properties to express torsional moments S_4 and S_{10}. These terms are written as

$$K_y = \oint_A z^4 dA, \qquad K_z = \oint_A y^4 dA, \qquad K_{zy} = \oint_A z^2 y^2 dA, \quad (8)$$

We can call these expressions "moments of inertia of second order". Another feature of the approach is that each nodal force is dependent on a symmetrical square matrix which includes terms composed only from the cross-sectional properties and constants. The non-linear influence of the other nodal displacements are excluded from the geometric nonlinear stiffness matrices. Therefore it is possible to separate the influences of different nodal displacements on the observed nodal force. This approach leads to the expression for each force which relies on the 6x6 matrices for the 3D bar element or 12 x 12 matrices for the 3D beam element.

2.3 The Non-linear solution for 3D members with the separate effects of deflections

The general equation for the forces at the end nodes of a 3D bar element is as follows:

$$S_i = \mathbf{k_{Ei}}\,\mathbf{U} + (\mathbf{U}^T\,\mathbf{h_i}\,\mathbf{U}) + u_j\,(\mathbf{U}^T\,\mathbf{q}\,\mathbf{U}) + u_j\,(\mathbf{U}^T\,\mathbf{g}\,\mathbf{U}) \qquad (9)$$

where index *j* relies on the index *i* of the evaluated force as *j=i+3* for *i=2,3* and *j=i-3* for *i= 5,6*

u_i, u_j ..... nodal displacements (scalar quantities) which have the major effect on the corresponding force S_i

k_{Ei} ..... i-th row of the elastic stiffness matrix,

$\mathbf{h_i}$ ..... square 6x6 matrices, which express the loading change during the load step (corresponds to the well known geometrical stiffness matrix $\mathbf{k_G}$)

U..... 6x1 vector of node displacements

$\mathbf{U}^T$..... transpose of vector U

q, g .....square 6x6 matrices which express the higher terms of order in the longitudinal strain energy of a bar

The expression results for a 3D beam element are more complicated. The derivation procedure is similar to that of a 3D bar element. The general equation for nodal forces applied to a 3D beam, which represent shear, axial force and bending, is

$$S_i = k_{Ei}\,\mathbf{U} + (\mathbf{U}^T\,{}^7\mathbf{h_i}\,\mathbf{U}) + (\mathbf{U}^T\,{}^1\mathbf{h_i}\,\mathbf{U}) \qquad (10)$$
$$+ u_i\,(\mathbf{U}^T\,{}^i\mathbf{e1}\,\mathbf{U}) + u_{i+6}\,(\mathbf{U}^T\,{}^{i+6}\mathbf{e2}\,\mathbf{U}) + u_j\,(\mathbf{U}^T\,{}^j\mathbf{e3}\,\mathbf{U}) + u_{j+6}\,(\mathbf{U}^T\,{}^{j+6}\mathbf{e4}\,\mathbf{U})$$

where ${}^7\mathbf{h_i} = -{}^1\mathbf{h_i}$ are square 12x12 matrices which express the loading change during the loading step (corresponds to, the well known, geometrical stiffness matrix $\mathbf{k_G}$). Superscript *7* or *1* express the influence of *7th* or *1st* node deflection as a major influence

k_{Ei} ..... corresponding row of the elastic stiffness matrix

U..... 12x1 vector of nodal displacements

${}^i\mathbf{e1}$, ${}^{i+6}\mathbf{e2}$, ${}^j\mathbf{e3}$, ${}^{j+6}\mathbf{e4}$ .. square 12x12 matrices which express the influence of higher order terms in the axial strain energy expression of a 3D beam element

u_i, u_j, u_{i+6}, u_{j+6}..... the node displacements (scalar quantities), which have a major influence on the corresponding force S_i, where index *i* is 2 and index *j* is 6 for the forces S_2, S_8, S_6, S_{12}, index *i* is 3 and index *j* is 5 for the forces S_3, S_9, S_5, S_{11},

Expressions for the torsional moments S_4, S_{10} are slightly different. These forces represent Saint Venant's torsion. The matrix equation for the nodal torsional moment is as follows:

$$S_i = \mathbf{k_{Ei}}\,\mathbf{U} + (\mathbf{U}^T\,{}^7\mathbf{h_i}\,\mathbf{U}) + (\mathbf{U}^T\,{}^1\mathbf{h_i}\,\mathbf{U}) + u_i\,(\mathbf{U}^T\,{}^i\mathbf{g1}\,\mathbf{U}) + u_{i+6}\,(\mathbf{U}^T\,{}^{i+6}\mathbf{g2}\,\mathbf{U}) \qquad (11)$$

where index *i* is either 4 or 10.

Matrices **g1** and **g2** for the torsional moment S_4, at the near end of the element include the same terms as matrices **g1** and **g2** for the torsional moment S_{10}, at the far end of the beam element, except they are of an opposite sign. The basic difference between the expressions for bending moments and shear forces is in the non-linear influence of the governing deflection u_i which is separated out of the matrix equation as a factor. The torsional moments are influenced only by the torsional deflection u_4 and u_{10}. Then the equation (10) or (11) can be expressed in a form

$$\mathbf{S} = \mathbf{S_E} + \mathbf{S_G} + \mathbf{S_Q} \qquad (12)$$

Forces $\mathbf{S_G}$ which corresponds to the forces which were calculated with the geometric stiffness matrix $\mathbf{k_G}$ are now divided into two parts $(\mathbf{U}^T\,{}^7\mathbf{h_i}\,\mathbf{U})$ and $(\mathbf{U}^T\,{}^1\mathbf{h_i}\,\mathbf{U})$. The first part $(\mathbf{U}^T\,{}^7\mathbf{h_i}\,\mathbf{U})$ express the influence of the deflections at the far end of the element to the solved nodal force S_i.

The second part ($\mathbf{U}^T\ {}^1\mathbf{h}_i\ \mathbf{U}$) express the influence of the deflections at the near end of the element to the solved nodal force S_i. For the force S_1 the matrix ${}^1\mathbf{h}_1 = \mathbf{0}$. Similarly for the force S_7 the matrix ${}^7\mathbf{h}_7 = \mathbf{0}$. For the force S_1 and S_7 are matrices ${}^7\mathbf{h}_1 = -{}^1\mathbf{h}_7$ and the terms remind in the geometrically stiffness matrix $\mathbf{k}_G$. Thus, the effect of the geometric non-linear behavior expressed by the approximate formula using the geometric stiffness matrix is good for axial force, but the other non-linear influences to the shear forces and bending and the torsional moments are not taken into the account in the equation (1).
Matrices ${}^i\mathbf{e1}, {}^i\mathbf{e2}, {}^i\mathbf{e3}, {}^i\mathbf{e4}$ for shear forces S_2 and S_8, and similarly for S_3 and S_9, include the same terms, however they are negative for ${}^i\mathbf{e1}, {}^i\mathbf{e2}, {}^i\mathbf{e3}, {}^i\mathbf{e4}$ for the forces S_8 and S_9 at the far end of the element. The same is true for the torsional moments S_4 and S_{10}. Therefore, only matrices ${}^i\mathbf{e1}, {}^i\mathbf{e2}, {}^i\mathbf{e3}, {}^i\mathbf{e4}$ need to be written to express the forces S_2 and force S_3. The matrices ${}^i\mathbf{e1}, {}^i\mathbf{e2}, {}^i\mathbf{e3}, {}^i\mathbf{e4}$ for the bending moments vary in a position and value of non zero elements. The following are matrix expressions showing the non linear relations between internal forces and deflections with respect to the governing deflections which are as factors out of the matrices.
The elastic matrix $\mathbf{k}_{Ei}$ in this expression can be submitted by the matrix with the influence of semirigid connections as was derived in [13]. We can therefore solve the member forces with respect to the non-linear behavior with included semirigid connections. The coefficients for the connections can be established either by experiments or by FEM calculation of a joint with respect to the material non-linear behavior. The simple iteration procedure described at the example at [6] could be applied for the solution.

2.4 The effect of the shear torsional energy

The influence on the geometrically non linear behavior due to the shear energy should be also included in the expression for the energy of the element. In the space framework the forces at any joint are distributed to the bending and the torsional moments. Also the torsional energy should be taken into the account. The space frame members are usually made from tubes. The Saint Venant torsion express properly the behavior of the member. Several basic assumptions are as folows. With respect to these assumptions the cross sections of the beam are not deformed, they are only rotated against each other under the Saint Venant torsion. For the position at axis x, e.g. $z_0 = 0$, $y_0 = 0$ we can write

$$\frac{\partial u_x}{\partial y} = 0, \frac{\partial u_x}{\partial z} = 0 \qquad \gamma_{zy} = 0 \qquad \frac{\partial u_x}{\partial y_0} = \frac{\partial u_x}{\partial z_0} = 0 \tag{13}$$

We can now write the expression for the rest of the shear stress tensor as follows

$$\gamma_{xy} = \frac{\partial u_y}{\partial x} + \frac{\partial u_x}{\partial x} \cdot \frac{\partial u_x}{\partial y} \qquad \gamma_{xz} = \frac{\partial u_z}{\partial x} + \frac{\partial u_y}{\partial x} \cdot \frac{\partial u_y}{\partial z} \tag{14}$$

Énergy of the deformed beam due to the shear deflections can be expressed at equation (15)

$$U = \frac{G}{2} \int_L \int_A \left[\left(\frac{\partial u_y}{\partial x}\right)^2 + \left(\frac{\partial u_z}{\partial x}\right)^2 + \left(\frac{\partial u_z}{\partial x} \cdot \frac{\partial u_z}{\partial y}\right)^2 + \left(\frac{\partial u_y}{\partial x} \cdot \frac{\partial u_y}{\partial z}\right)^2 + 2\left(\frac{\partial u_y}{\partial x}\right)\left(\frac{\partial u_z}{\partial x} \cdot \frac{\partial u_z}{\partial y}\right) + 2\left(\frac{\partial u_z}{\partial x}\right)\left(\frac{\partial u_y}{\partial x} \cdot \frac{\partial u_y}{\partial z}\right) \right] dx\, dA \tag{15}$$

After the same procedure which was shown and explained above, we will receive matrix expression for the nodal forces with respect to the energy spent for the shear deformation due to the Saint Venant torsion. The values of terms in the matrices are similar to the values at the stiffness matrix with respect to the axial deformation. For the materials with relatively large shear modulus is therefore reasonable to include the effect to the analysis. Final matrix equation for the nodal forces is different for the forces due to the shear and bending and different for the forces due to

the torsion S_4, and S_{10}. This fact is similar as at the previous equations (10) and (11). We can write for the first group of the forces the equation (16)

$$\mathbf{S} = \frac{GA}{2} \{ \mathbf{e}\ \mathbf{U} + \tfrac{1}{3} \mathbf{e}\ \mathbf{U}\ \mathbf{U}^T\ \mathbf{c}\ \mathbf{U} \} \tag{16}$$

and for the torsional forces we have

$$S_4 = \frac{GA}{2}\ {}^4\mathbf{d}\ \mathbf{U}\ \mathbf{U}^T\ \mathbf{r}\ \mathbf{U}, \qquad S_{10} = \frac{GA}{2}\ {}^{10}\mathbf{d}\ \mathbf{U}\ \mathbf{U}^T\ \mathbf{r}\ \mathbf{U}, \tag{17}$$

These expressions can be added to the equation (12) and solved simultaneously. The orthogonal transformation from the local to the global system can be used to express the non-linear expression for the whole system.

Conclusion

The derived equations allow to obtain geometric non-linear solution of an arbitrary 3D beam system with the possibility to solve effect of each deflection component separately. The accuracy of the solution can be easily controlled according to which matrices are used. The stability of large one-layer systems is highly effected by the real rigidity of nodes, which can be partially plastified. The derived equations allow to solve 3D system with respect to the non-linear behavior with the effect of the semirigid connection. The evaluation of the effect of each deflection to the non-linear behavior of system is assume to be done with respect to different topology of space systems.

References

[1] J.S. Przemieniecki, Theory of Matrix Structural Analysis, Mc Graw Hill, (1968)
[2] Y. Goto and W. F. Chen, Second- Order Elastic Analysis for Frame Design, J. of Struct. Eng. ASCE, Vol. 113, 7, July, 1501-1529, (1987)
[3] J.Y. Richard Liew and W. F. Chen, Stability Design of Semirigid Frames, John Willey & Sons Inc., New York, (1996)
[4] H. Nooshin , Third International Conference on Space Structures, Elsevier Ap plied Science Publishers, London, New York, (1984)
[5] G. A. R. Parke and C. M. Howard, Space Structures 4 th Conference Proceedings on Space Structures , Thomas Telford Services Ltd. London , (1993)
[6] M. Vasek, Solution of Bars or Beams with repect to Geometrical Nonlinearity, Stavebnicky časopis VEDA, Vol.24, 5, 415- 428, Vyd. Slovenskej Akademie Vied, Bratislava, (1975)
[7] M. Vasek, The Non-linear Behaviour of Large Space Bar and Beam Structures, G.A.R. Parke and C.M.Howard, Space Structures 4 th Conference Proceedings on Space Structures , 665-674, Thomas Telford Services Ltd. London, (1993)
[8] M. Vasek, M. Drdacky, K. Hoblik, Research Report of the Czech Grant Office no. 103/93/2027 , Space Roof Structural System, Pittsburgh, Prague, (1996)
[9] I. H.J. Toader, Stability functions for Members with Semirigid Joint Connections, J. of Struct. Eng., Vol.119, 2, February, ASCE, 505-521, (1993)
[10] M.A.M.Torkamani, M.Sonmez, J.Cao,Second-Order Elastic Plane-Frame Analysis Using Finite Element Method,J. of Struct. Eng., Vol.123, 9 , Sept, ASCE, (1997)

The Finite Strip Method in Computational Engineering

Dragan D. MILASINOVIC
Assoc. Dean
Faculty of Civil Eng.
Subotica, Yugoslavia

Dragan D. Milasinovic, born 1954, received his Civil Eng. degree from the Univ. of Sarajevo in 1978 and Ph.D. in 1987. He is currently a faculty member at the Univ. of Novi Sad where he is an Assoc. Prof. of Plates and Shells Theory.

Summary

In the last two decades the Finite Strip Method (FSM) has been successfully introduced in the studies of linear behavior, vibrations and buckling as well as nonlinear behavior of various types of prismatic folded plates and curved shells. The reason for the introduction of this method lies in the fact that resolving of several classes of practical problems it is much faster than the more comprehensive and adaptable Method of Finite Elements (FEM). This is generally valid for structures with regular geometrical shape and simple boundary conditions, whose discretization into many finite elements is often very expensive. In such cases the FSM can be extremely competitive in terms of cost and accuracy, both during calculations and in practical application. Discretization of the cross-section into a mesh of finite strips enables the adoption of a finite number of degrees of freedom in the section.

1. The Finite Strip Variational Formulation

The well-known basic procedure of the method is the discretization of plate structures into longitudinal strip elements. The general form of the finite strip displacement function is approximated by the product of polynomes and series which is an interpolation between the classical Ritz and the FEM,

$$f = \sum_{m=1}^{r} Y_m(y) \cdot \sum_{k=1}^{c} \mathbf{N}_k(x) \cdot \mathbf{q}_{km} \qquad (1)$$

where $Y_m(y)$ are functions from the Ritz and $\mathbf{N}_K(x)$ are interpolation functions from the FEM. According to the Green-Lagrange's strain tensor, we present the strain components in an arbitrary point, on the distance z from the middle plane of the plate, as functions of the displacement components of the point of the middle plane of the plate (u_0, v_0, $w=w_0$), as follows:

$$\begin{aligned}
\varepsilon_x &= u_{o,x} + \frac{1}{2}\left(u_{o,x}^{\ 2} + w_{,x}^{\ 2}\right) - z \cdot w_{,xx}, \\
\varepsilon_y &= v_{o,y} + \frac{1}{2}\left(u_{o,y}^{\ 2} + w_{,y}^{\ 2}\right) - z \cdot w_{,yy}, \qquad (2) \\
\gamma_{xy} &= u_{o,y} + v_{o,x} + u_{o,y} \cdot u_{o,x} + w_{,x} \cdot w_{,y} - 2 \cdot z \cdot w_{,xy}
\end{aligned}$$

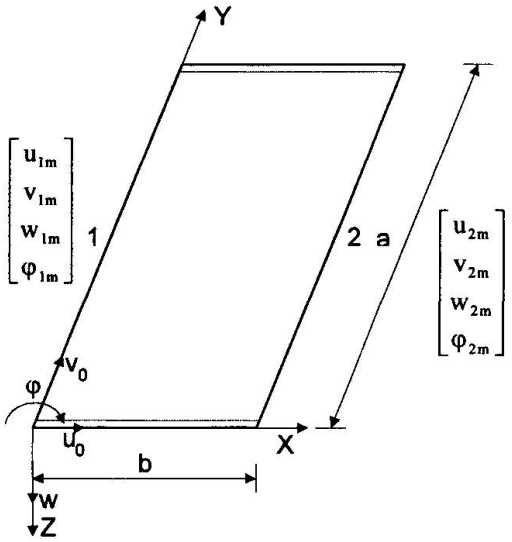

Fig. 1 A finite strip with eight degrees of freedom

The previous expressions can be obtained as products of the following matrices and vectors:

$$\mathbf{e}_o = \mathbf{L}_1\mathbf{A}_u \cdot \mathbf{q}_u = \mathbf{B}_{u1} \cdot \mathbf{q}_u$$

$$\eta_o = \frac{1}{2}\mathbf{L}_1\tilde{\mathbf{A}}_w \cdot \mathbf{W} \cdot \mathbf{L}_2\mathbf{A}_w \cdot \mathbf{q}_w = \frac{1}{2}\mathbf{B}_{w1} \cdot \mathbf{W} \cdot \mathbf{B}_{w2} \cdot \mathbf{q}_w$$

$$\xi_o = \frac{1}{2}\mathbf{L}_1\tilde{\mathbf{A}}_u^u \cdot \mathbf{U} \cdot \mathbf{L}_2\mathbf{A}_u^u \cdot \mathbf{q}_u^u = \frac{1}{2}\mathbf{B}_{u1}^u \cdot \mathbf{U} \cdot \mathbf{B}_{u2}^u \cdot \mathbf{q}_u^u$$

$$\kappa = \mathbf{L}_3\mathbf{A}_w \cdot \mathbf{q}_w = \mathbf{B}_{w3} \cdot \mathbf{q}_w$$

$$\mathbf{e}_0^{\mathrm{I}} = \mathbf{L}_4\mathbf{A}_u^u \cdot \mathbf{q}_u^u = \mathbf{B}_{u4}^u \cdot \mathbf{q}_u^u$$

$$\mathbf{e}_0^{\mathrm{II}} = \mathbf{L}_5\mathbf{A}_u^v \cdot \mathbf{q}_u^v = \mathbf{B}_{u5}^v \cdot \mathbf{q}_u^v \qquad (3)$$

Where:

$$\mathbf{e}_o = \begin{bmatrix} u_{o,x} \\ v_{o,y} \\ u_{o,y} + v_{o,x} \end{bmatrix}, \quad \mathbf{e}_o^{\mathrm{I}} = \begin{bmatrix} u_{o,x} \\ 0 \\ u_{o,y} \end{bmatrix}, \quad \mathbf{e}_o^{\mathrm{II}} = \begin{bmatrix} 0 \\ v_{o,y} \\ v_{o,x} \end{bmatrix},$$

$$\eta_o = \begin{bmatrix} \frac{1}{2}w_{,x}^{\,2} \\ \frac{1}{2}w_{,y}^{\,2} \\ w_{,x} \cdot w_{,y} \end{bmatrix}, \quad \xi_o = \begin{bmatrix} \frac{1}{2}u_{o,x}^{\,2} \\ \frac{1}{2}u_{o,y}^{\,2} \\ u_{o,x} \cdot u_{o,y} \end{bmatrix}, \quad \kappa = \begin{bmatrix} -w_{,xx} \\ -w_{,yy} \\ -2w_{,xy} \end{bmatrix},$$

$$\mathbf{L}_1 = \begin{bmatrix} \frac{\partial}{\partial x} & 0 \\ 0 & \frac{\partial}{\partial y} \\ \frac{\partial}{\partial y} & \frac{\partial}{\partial x} \end{bmatrix}, \quad \mathbf{L}_2 = \begin{bmatrix} \frac{\partial}{\partial x} \\ \frac{\partial}{\partial y} \end{bmatrix}, \quad \mathbf{L}_3 = \begin{bmatrix} -\frac{\partial^2}{\partial x^2} \\ -\frac{\partial^2}{\partial y^2} \\ -2\frac{\partial^2}{\partial x \partial y} \end{bmatrix}, \qquad (4)$$

$$\mathbf{L}_4 = \begin{bmatrix} \frac{\partial}{\partial x} \\ 0 \\ \frac{\partial}{\partial y} \end{bmatrix}, \quad \mathbf{L}_5 = \begin{bmatrix} 0 \\ \frac{\partial}{\partial y} \\ \frac{\partial}{\partial x} \end{bmatrix},$$

$$\mathbf{A}_u = \begin{bmatrix} \mathbf{A}_u^u & 0 \\ 0 & \mathbf{A}_u^v \end{bmatrix}, \quad \mathbf{q}_u = \begin{bmatrix} \mathbf{q}_u^u \\ \mathbf{q}_u^v \end{bmatrix}, \quad \tilde{\mathbf{A}}_w = \begin{bmatrix} \mathbf{A}_w & 0 \\ 0 & \mathbf{A}_w \end{bmatrix},$$

$$\mathbf{W} = \begin{bmatrix} \mathbf{q}_w & 0 \\ 0 & \mathbf{q}_w \end{bmatrix}, \quad \tilde{\mathbf{A}}_u^u = \begin{bmatrix} \mathbf{A}_u^u & 0 \\ 0 & \mathbf{A}_u^u \end{bmatrix}, \quad \mathbf{U} = \begin{bmatrix} \mathbf{q}_u^u & 0 \\ 0 & \mathbf{q}_u^u \end{bmatrix}.$$

The total potential energy is defined as the sum of the potential energy of external forces and the strain energy. The formulation of strip characteristics will be presented using the principle of minimum total potential energy.

1.1 Geometrically Nonlinear Viscoelastic Problems

In the non-homogeneous finite strip composed of the layers of concrete and reinforcement, the conditions of balance represent a system of geometrically nonlinear equations.

$$\left[\hat{\mathbf{K}}(t) + \tilde{\mathbf{K}}(t)\right] \cdot \mathbf{q}(t) = \mathbf{D}_o(t) \cdot \left[\hat{\mathbf{K}}(t_o) + \tilde{\mathbf{K}}(t_o)\right] \cdot \mathbf{q}(t_o) + \mathbf{Q}, \qquad (5)$$

where $\hat{\mathbf{K}}$ is the classical or basic stiffness matrix, $\tilde{\mathbf{K}}$ the geometrical stiffness matrix.

1.2 Geometrically Nonlinear Elastic Problems

As the instant strains are elastic Eq. (5) can be written in the form:

$$\left[\hat{\mathbf{K}}(t_o)+\tilde{\mathbf{K}}(t_o)\right]\cdot\mathbf{q}(t_o)=\mathbf{Q}_o. \qquad (6)$$

This is a system of non-linear simultaneous equations at time $t=t_0$.

1.3 Linear Elastic Problems

By exclusion of the geometrical stiffness matrix from the above equation we obtain a linear system of differential equation.

$$\hat{\mathbf{K}}(t_0)\cdot\mathbf{q}(t_0)=\mathbf{Q}_0. \qquad (7)$$

1.4 Linear Viscoelastic Problems

The behavior of the material, which changes with time, can be approximation by the following equations of balance

$$\hat{\mathbf{K}}(t)\cdot\mathbf{q}(t)=\mathbf{D}_0(t)\cdot\mathbf{Q}_0+\mathbf{Q} \qquad (8)$$

which is a system of linear simultaneous equations, which enclose time dependent effects.
The basic stiffness matrix blocks, together with the geometrical stiffness matrix blocks are used in this interactive analysis:

$$\hat{\mathbf{K}}(t)=\begin{bmatrix}\hat{\mathbf{K}}_{uu} & \frac{1}{2}\hat{\mathbf{K}}_{uw}\\ \frac{1}{2}\hat{\mathbf{K}}_{wu} & \hat{\mathbf{K}}_{ww}\end{bmatrix},$$

$$\tilde{\mathbf{K}}(t)=\left[\begin{array}{c|c}0 & \frac{1}{4}\tilde{\mathbf{K}}_{uw}\\ \hline \frac{1}{2}\tilde{\mathbf{K}}_{wu} & \begin{array}{l}\frac{1}{2}\tilde{\mathbf{K}}_{ww}+\\ \frac{3}{4}\tilde{\mathbf{K}}^{*}_{ww}+\\ \frac{3}{4}\tilde{\mathbf{K}}^{**}_{ww}\end{array}\end{array}\right]+\left[\begin{array}{c|c}0 & \begin{array}{l}\frac{1}{4}\tilde{\mathbf{K}}^{u}_{uw}+\\ \frac{1}{2}\tilde{\mathbf{K}}^{u*}_{uw}\end{array}\\ \hline \begin{array}{l}\frac{1}{4}\tilde{\mathbf{K}}^{u}_{wu}+\\ \frac{1}{4}\tilde{\mathbf{K}}^{u*}_{wu}\end{array} & 0\end{array}\right]+$$

$$+\left[\begin{array}{c|c}\begin{array}{l}\frac{1}{2}\tilde{\mathbf{K}}^{uu}_{uu}+\\ \frac{3}{4}\tilde{\mathbf{K}}^{uu*}_{uu}+\\ \frac{3}{4}\tilde{\mathbf{K}}^{uu**}_{uu}\end{array} & \frac{1}{2}\tilde{\mathbf{K}}^{uv}_{uu}\\ \hline \frac{1}{4}\tilde{\mathbf{K}}^{vu}_{uu} & 0\end{array}\right] \qquad (9)$$

Since the system of equations is nonlinear, the equations of balance in any step of the iterative procedure resolving will not be satisfied. Due to this fact, we shall have the vector of non-balanced forces, i.e., residual loading. It is favorable to present this vector separately for the linear and nonlinear part.

$$\mathbf{R}=\hat{\mathbf{R}}+\tilde{\mathbf{R}}-\mathbf{Q}, \qquad (10)$$

$\mathbf{Q}$ is the load vector and $\mathbf{q}$ the vector of nodal line displacement parameters for the finite strip.

$$\mathbf{Q}=\begin{bmatrix}\mathbf{Q}_u\\ \mathbf{Q}_w\end{bmatrix},\ \mathbf{q}=\begin{bmatrix}\mathbf{q}_u\\ \mathbf{q}_w\end{bmatrix}, \qquad (11)$$

2 Newton-Raphson's iterative procedure of solution

The variational statement about stationary of the total potential energy in nonlinear problems results in a vector of non-balanced forces,

$$\mathbf{R}=\left[\Phi_{,\mathbf{q}^T}\right]=\left[\hat{\mathbf{K}}+\tilde{\mathbf{K}}\right]\cdot\mathbf{q}-\mathbf{Q}=\mathbf{0}, \qquad (12)$$

Taylor's expansion of (12) gives:

$$\mathbf{R}_1=\mathbf{R}(\mathbf{q}_0+\delta_0)=\mathbf{R}(\mathbf{q}_0)+\overline{\mathbf{K}}_0\delta_0+\ldots= \qquad (13)$$
$$\mathbf{R}_0+\overline{\mathbf{K}}_0\cdot\delta_0+\ldots$$

where $\overline{\mathbf{K}}_0=\mathbf{R}_{,\mathbf{q}}$ is the second partial derivative of Φ calculated at $\mathbf{q}_0$ (tangent stiffness matrix).

If (13) is zero and if only the linear terms in $\mathbf{q}_0$ are considered the standard Newton-Raphson iteration is obtained:

$$\delta_0=-\overline{\mathbf{K}}_0^{-1}\cdot\mathbf{R}_0. \qquad (14)$$

Using this approach, an iteration further gives:

$$\delta_n=-\overline{\mathbf{K}}_n^{-1}\cdot\mathbf{R}_n, \qquad (15)$$

where $\overline{\mathbf{K}}_n = \mathbf{R}_{,q}$ at $\mathbf{q}_n$.

The criterion for convergence, based on the residual force values, is:

$$\frac{\sqrt{\sum_{i=1}^{N}\left(\mathbf{R}_i^n\right)^2}}{\sqrt{\sum_{i=1}^{N}\left(\mathbf{Q}_i\right)^2}}\cdot 100 \le \varepsilon \ , \qquad (16)$$

where N is the total number of nodal lines of the decomposed structure, and rt. determines the number of iteration. This criterion means that convergence occurs when the norm of residual forces becomes lesser than ε, which is assigned.

3 Examples

3.1 Example 1

This example presents a comparative analysis of calculations of a prestressed concrete element according to the theory of prestressed concrete within a line analysis, and to the FSM. The results differ considerably, due to two main reasons. First, by the FSM, as opposed to the classical calculation based on the theory of line girders, we can obtain the stress-strain state of the thin-walled bar with open and deformable cross-section. Second, in the calculation of the stress-strain state in an arbitrary time t, the Poynting-Thompson's model of viscoelastic body is used.
Figure 2 presents the cross-section of prestressed concrete element, with the length of 10.20 m.

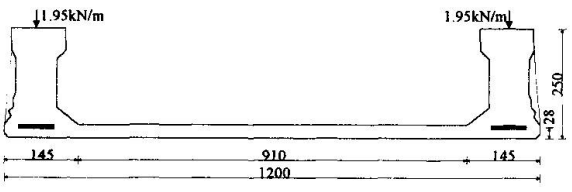

Fig. 2 Cross-section of prestressed concrete element

The element is made of C60, and it is prestressed adhesively with four cables 7ϕ5mm, with total area of 5.5 cm^2 and total initial prestresing force of 667.2 kN. The allowed stress in steel is $128x10^4$ kN/m^2, and the elasticity modulus of steel is $E_t=2x10^8$ kN/m^2.
Characteristics of concrete as a viscoelastic material are:

$$E_c = E_{28} = 4.138\cdot 10^7 \ kN/m^2,$$
$$\varphi(t_\infty, t_o) = 2.8,$$
$$\chi(t_\infty, t_o) = 0.75,$$
$$\sigma^p_{allowed} = -18500 \ kN/m^2,$$
$$\sigma^t_{allowed} = 2200 \ kN/m^2.$$

Apart from the own weight, the element is subject to live loading which is transmitted to the longitudinal beams. This loading is considered to be movable, and it does not induce the effects of concrete creep. The loading on two beams is 3.9 kN/m. In combination with the own weight, if it is also considered as line loading, the loading on both beams is 6.0 kN/m. Figure 3. presents the mesh of finite strips with the corresponding boundary conditions.

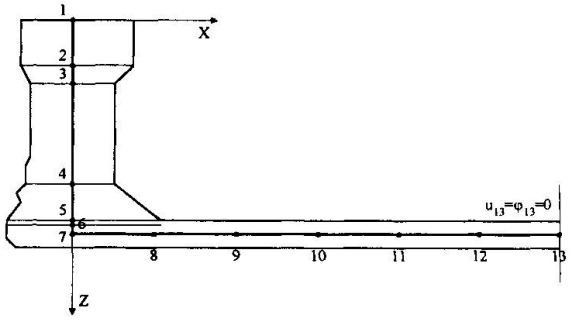

Fig. 3 Mesh of finite strips and symmetry conditions

The results of calculation are presented in Figure 4 (a), (b) and (c). In Figure 4(a) the diagram drawn in the full line represents σ_y caused by own weight and prestressing in the time t_0, while the dotted line is for the time t_∞. The stresses are calculated in the middle of the span length. Figure 4(b) presents the diagram of σ_y caused by the live loading, and Figure 4(c) of that caused by the total loading and prestressing in the time t_∞.
It can be seen that the stresses in the concrete exceed the allowed values. The line analysis, which can not yield good results for such a cross-section, gives stress values which are within the allowed limits. According to this calculation, in the upper

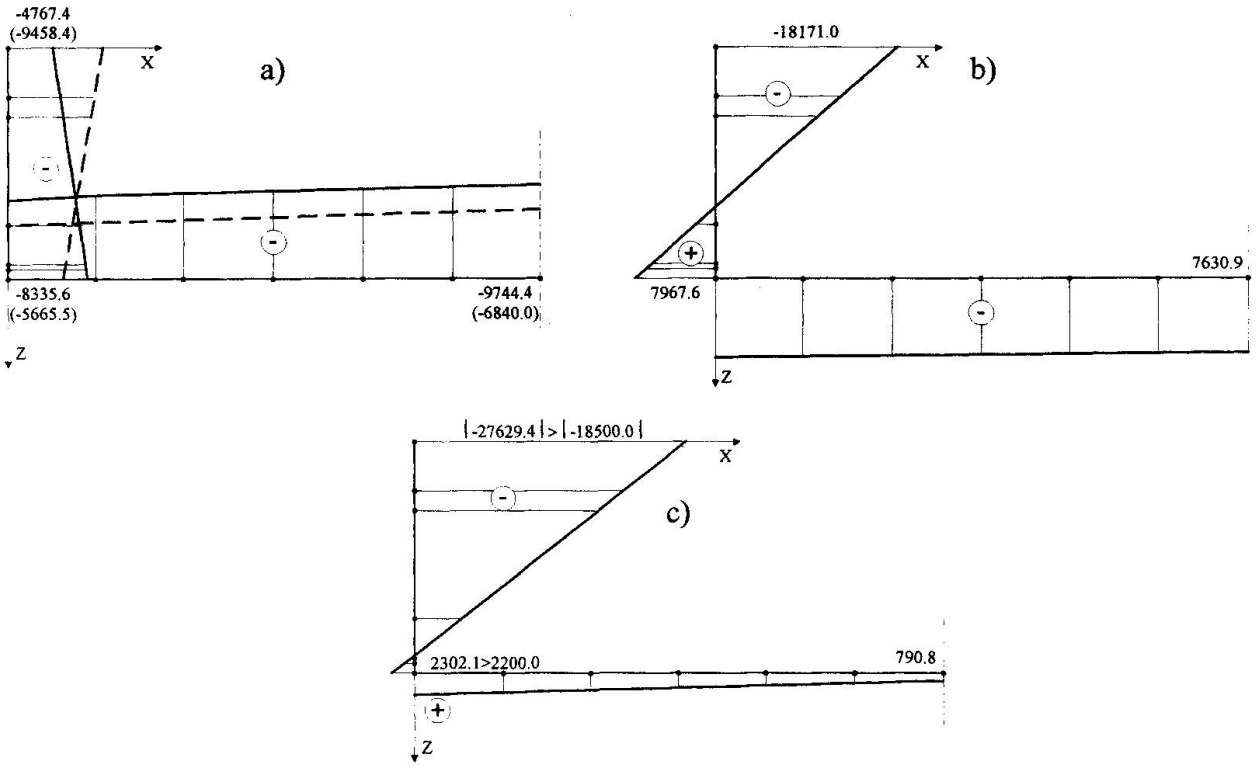

Fig. 4 Diagrams of stress σ_y in the middle of girder span length, (a) effect of own weight and prestressing in t_0 and t_∞, (b) effect of live loading, (c) effect of own weight, prestressing and live loading in t_∞

fibre σ_y^p = -18310 kN/m^2, and in the lower fibre σ_y^t = 616 kN/m^2.
In addition, it should be noted that according to the FSM, the loss of prestressing force caused by elastic strains of concrete (3.23%) and elastic strains and creep of concrete (6.99%) is much lesser than the total prestressing force loss anticipated in the calculation according to the line analysis (20%).

3.2 Example 2

Prefabricated prestressed concrete girders are complex elements, 75 x 210 cm, lightened by three openings ϕ50 cm. The elements are from 13.40 to 25.40 m long, see Figure 5 and they serve as bridge girders. They are made of the following materials:

- steel for prestressing 1800/1600, with nominal cross-section of 0.93 cm^2,
- concrete C40.

The cutting of tendons can be carried out only when the concrete reaches the strength of 30 MN/m^2. The reason for this is the unfavorable stress state of the girder in the moment of prestressing. Here we shall

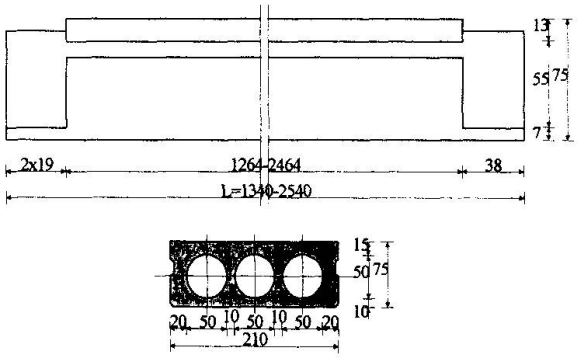

Fig. 5 View and cross-section of bridge girder

analyze a girder, which is 19.50m long, prestressed with 48 tendons with total area of 44.64 cm^2, and total initial prestressing force of 5625 kN.
The mesh of finite strips in the cross-section

of the girder is presented in Figure 6. Polyhedral shell finite strips with eight degrees of freedom were used. Eleven terms of the series were used in the calculation of own weight and prestressing.

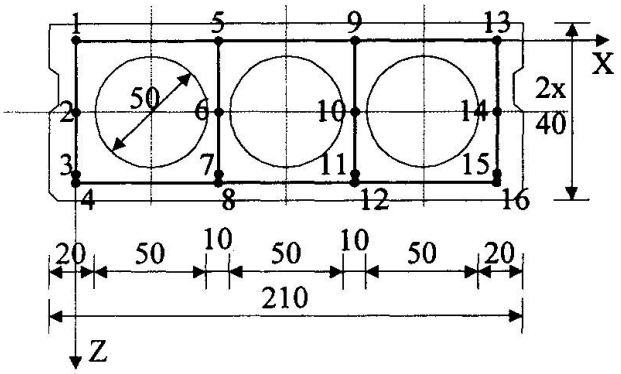

Fig. 6 Mesh of finite strips in the cross-section of girder

Figure 7 presents the most unfavorable distribution of the stress σ_y in the node lines 1 and 3. Tension stress is unfavorable for node line 1, and high stress of pressure for node line 3

displacement amplitudes. Complex mathematical expressions were programmed within the frame of the standard Newton-Raphson's iterative procedure. The application of the FSM promises more reliable results than the application of the FEM, since the errors of discretization in the former method are much lesser. Bearing in mind that the FSM is a semi-analytical and semi-numerical method, in the theory of polyhedral shells, we find it very favorable in solving of this problem.

References

1. Cheung, Y.K., "The Finite Strip Method in Structural Analysis", Oxford, Pergamon Press, 1976.
2. Loo, W.C., Causeus, A.R., "The Finite Strip Method in Bridge Engineering", Wexham Springs, Viewpoint Publications (C&CA), 1978.
3. Milašinović, D.D., "The Finite Strip Method in Computational Mechanics, Faculty of Civil Engineering: Subotica, Budapest, Belgrade, 1997

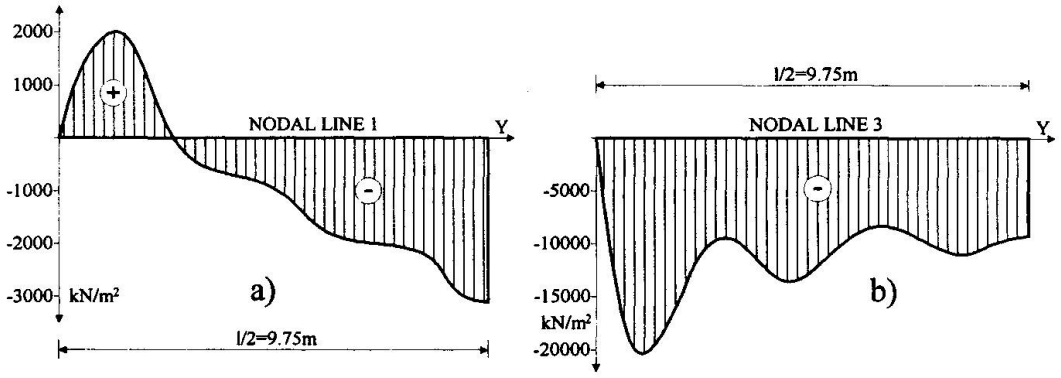

Fig. 7 Distribution of stress σ_y (kN/m^2); (a) in node line 1, (b) in node line 3

5 Conclusions

A nonlinear FSM has been presented for use in the design of reinforced concrete plate structures. The procedure has advantages over the conventional FEM, since the application of numerical integration is avoided, and the stiffness matrices, loading vectors and residual forces are expressed explicitly as a function of the nodal

Strength Optimisation and Crack Resistance of RC Structures

Yuriy M. POCHTMANN
Prof.
Dnepropetrovsk State Univ.
Dnepropetrovsk, Ukraine

Yuriy M. Pochtman, born 1934, Dr Sc, Prof. of Dept of Applied Mathematics and Mechanics, Dnepropetrovsk State University. Member of New York Academy of Sciences and IABSE.

Summary.

The calculation of strength for reinforced concrete members is at present executed pursuant to requirements [1], where for efforts each of combinations in sections, in view of position of the section relatively to longitudinal axis of member (normal, inclined, spatial) the appropriate formulas for calculation of strength are adduced. The aid [2], made in development of [1], contains the auxiliary tables oriented on «hand-operated» calculations. However such approach is badly combined with opportunities of computer simulation.

1. Optimum Formulation

At the same time, all problems of calculation of strength, submitted in [1] and [2] have sufficient generality, as follows: in each of them, at given efforts, overall dimensions of section, classes of concrete and reinforcement, it is necessary to find the minimum area of reinforcement at which the conditions of strength, as well as parametrical and structural restrictions, intended in [1], are provided. Such formulation of the problem of calculation of strength quite correspondents to the problem of nonlinear mathematical programming (NMP), as it represented, for example, in [3]:

$$\min\left\{F(\bar{x}) \middle| g_i(\bar{x}) \geq 0, i = 1,..q; h_j(x) = 0, j = 1,..,P\right\}. \qquad (1)$$

Here: $\bar{x} = x_i(1,..,n)$ - n-dimensional the vector of unknown variables; $\Phi(\bar{x})$ - scalar, in general case - nonlinear functions of all several variables x_i; $g_i(\bar{x}), h_j(\bar{x})$ - scalar, in general case - nonlinear functions of all or some variables forming system of restrictions, correspondingly, in form of unequations and equations.

It is important to note that formalization of wide class of strength problems in form of optimization model [1] permits during the construction of appropriate computing algorithms to use enough general dependencies which describes stress-strained state of reinforcement and concrete in section, without additional simplifications, stipulated by the limited opportunities of «hand-operated» calculation.

This article enters the improved diagram of dependence of stress in longitudinal reinforcement σ_s from the relative depth of compressed zone of concrete ξ for bending and eccentric com-

pressed members from concrete having class B30 and below, with reinforcement of class A-I, A-II, A-III (see fig.1, curve 1). The stress σ are described by not direct but broken line in segment $\xi \in [\xi_R, 1]$ with point of inflection in {} in contrast to known simplified diagram, adduced in [4] and used in [1]. By this it is provided the better coincidence with exact formula of stress [4].

Here: $\bar{\sigma} = \frac{\sigma_s}{R}$-reduced stress in reinforcement placed at extended or less compressed edge of member.

Beside it is used a single expression for determination of stresses in longitudinal reinforcement

$$\sigma_s = R_s \cdot F(\xi), \xi \in [0,1.1] \qquad (2)$$

where $F(\xi)$ - function, approximated the considered diagram. The interpolation polinom of 6-th degree is applied as such function.

$$F(\xi) = a_0 + \sum_1^6 a_i \xi^i \qquad (3)$$

Values of coefficients $a_i (i = 0,..,6)$ for classes of concrete B12,5 and B15 by $\gamma_{B2} = 0,9$ are calculated on computer and listed in table.

Table.

a_i	Class of Concrete	
	B12.5	B15
a_0	0.987019	0.987970
a_1	3.036522	2.868721
a_2	-36.030163	-34.394078
a_3	140.012541	135.665211
a_4	-224.673126	-222.200063
a_5	149.077017	151.287490
a_6	-33.430986	-35.232187

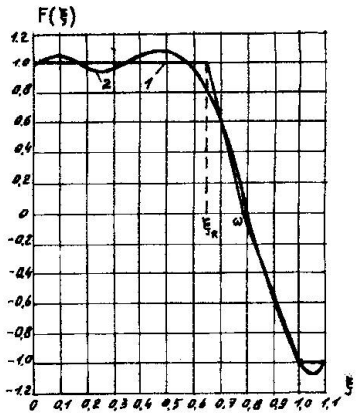

fig 1.

The diagram $F(\xi)$, having been received for concrete B15, is represented on fig.1 (curve 2).

Let's consider some problems of calculations of reinforced concrete members formulating as a problem of NMP using dependencies (2) and (3). All the designations, except of specially mentioned, are accepted from [2].

2. The strength calculation for normal sections of bended members

The relative depth of compressed zone of concrete, as well as tensioned and compressed areas of reinforcement are accepted as unknown variables of the NMP problem:

$x_1 \equiv \xi, x_2 \equiv As, x_3 \equiv A's$. The NMP problem accepts the following air:

Find the minimum of object-function:

$$\min \Phi(x) = x_2 + x_3 \tag{4}$$

by executing of:

a) conditions of strength

$$x_1(1 - 0.5x_1) + \frac{x_3 R_s (h_0 - a')}{R_B b h_0^2} - \frac{M}{R_B b h_0^2} \geq 0 \tag{5}$$

b) equation of balance

$$\frac{\left(x_2\left(a_0 + \sum_1^6 a_i x_1^i\right) - x_3\right)}{x_1} - \frac{R_B b h_0}{R_s} = 0 \tag{6}$$

c) parametrical and structure restrictions

$$\left.\begin{aligned} &x_1 > 0, \\ &x_1 < 1.1, \\ &x_2 - 0.0005bh0 \geq 0, \\ &x_3 \geq 0. \end{aligned}\right\} \tag{7}$$

Solutions of problem (4)-(7) is illustrated by control examples taken from [2].

The example 1: b=30cm; h=80cm; a=5cm; a′ =3cm; concrete B15 ($\gamma_{B2} = 0{,}9$); reinforcement AIII; M=20.0 toneforce · m. The results (the correspondenced values from [2] are indicated in brackets):

$x_1 \equiv \xi = 0.323(0.322)$; $x_2 \equiv A_s = 11.36(11.34)\text{cm}^2$

The example 2: b=30cm; h=80cm; a=5cm; a′ =3cm; concrete B15 ($\gamma_{B2} = 0{,}9$); reinforcement AIII; M=80.0 toneforce · m. The results :

$x_1 \equiv \xi = 0.538(0.550)$; $x_2 \equiv A_s = 35.96(35.91)\text{cm}^2$; $x_3 \equiv A_s' = 10.62(10.00)\text{cm}^2$.

3. The strength calculation for eccentric stressed members

Unknown variables of the NMP problem are accepted as in previous example:

$x_1 \equiv \xi; x_2 \equiv A_s; x_3 \equiv A_s'$.

The object-function has a previous air and conditions of strength is presented as:

$$\frac{2(R_B b h_0^2 x_1 (1 - 0.5x_1) + R_s (h_0 - a') \cdot x_3)(K_1 + K_2 (x_2 + x_3) - N)}{2e_0 (K_1 + K_2 (x_2 + x_3)) + (h_0 - a')(K_1 + K_2 (x_2 + x_3) - N)} \geq N \tag{8}$$

Here :

$$K_1 = \frac{1.6 E_B b h}{3\left(\frac{l_0}{h}\right)^2 \varphi_1}\left(\frac{0.11}{0.1 + \delta_e} + 0.1\right),$$

$$K_2 = \frac{1.6E_S}{\left(\frac{l_0}{h}\right)^2}\left(\frac{h_0 - a'}{h}\right)^2,$$

Then the equation of balance is:

$$\left(x_2\left(a_0 + \sum_1^6 a_i x_1^i\right) - x_3\right) + \frac{N}{R_S x_1} - \frac{R_B b h_0}{R_S} = 0 \qquad (9)$$

Parametrical and structure restrictions are recorded as

$$\left.\begin{aligned} &x_1 > 0, \\ &x_1 \le 1.1, \\ &x_2 - 0.0005bh_0 \ge 0, \\ &x_3 - 0.0005bh_0 \ge 0. \end{aligned}\right\} \qquad (10)$$

It is accepted that in case of symmetric reinforcement $x_2 = x_3$ in problem (4),(8)-(10).
The example 3: b=40cm; h=60cm; a=a′ =4cm; concrete B25
($\gamma_{B2} = 0,9$); $l_0 = 6.0$m; $N_1 = 70.0$tonforce; $E_B = 275000$kgforce / cm^2; reinforcement AIII;
$M_1 = 21.3$toneforce · m.. The results (value from [2] are in brackets):
$x_1 \equiv \xi = 0.235(0.235)$; $x_2 = x_3 \equiv A_s = 6.51(7.6)$cm^2;

4. The strength calculation of inclined sections of bended members

The length of projection of inclined crack $C_0 \equiv x_1$, the length of projection of inclined section $C \equiv x_2$ and the area of cross reinforcement within the limits of inclined crack, referred to space of cross bars $\frac{A_{sw}}{S} \equiv x_3$ are accepted as unknown variables of the NMP problem.
The NMP problem has the following air:
The object-function:

$$\min \Phi = x_1 \cdot x_3 \qquad (11)$$

condition of strength:

$$\frac{(1+\varphi_f)\varphi_{B2}R_{Bt}bh_0^2}{x^2} + R_{sw} \cdot x_1 x_3 + q_1 \cdot x_2 - Q_{max} \ge 0 \qquad (12)$$

restriction on maximal value of $Q_B \le Q_B^{max}$:

$$x_2 - \frac{\varphi_{B2}h_0}{2.5} \ge 0 \qquad (13)$$

restriction on minimum value of $Q_B \ge Q_B^{min}$:

$$x_2 - \frac{\varphi_{B2} h_0}{\varphi_{B3}} \le 0 \qquad (14)$$

restriction on minimum of web reinforcement:

$$x_3 - \frac{(1+\varphi_f)\varphi_{B3} R_{Bt} b}{2R_{SW}} \ge 0 \qquad (15)$$

restrictions on value of C_0:

$$x_2 - x_1 > 0 \qquad (16)$$

$$x_1 - \frac{\varphi_{B2} h_0}{2.5} \ge 0 \qquad (17)$$

$$x_1 - 2h_0 \le 0 \qquad (18)$$

and, at least, condition of equality $Q_B = Q_S$:

$$\frac{x_1^2 x_3 - (1+\varphi_f)\varphi_{B2} R_{Bt} b h_0^2}{R_{SW}} = 0 \qquad (19)$$

The example 4: b=20cm; h=40cm; a=3cm;concrete B15;
($\gamma_{B2} = 0{,}9$); cross reinforcement A-I;
$Q_{max} = 13.75$ tonforce;
$q_1 = 3.2$ tonforce / m.
The results (value from [2] are in brackets):
$x_1 \equiv C_0 = 45.2(44.8)\text{cm}^2$; $x_2 \equiv C = 107(108)$cm;
$x_3 \equiv A_{SW} / S = 0.07(0.07)\text{cm}^2 / \text{cm}$.

Conclusions

As is obviously, the results of solution of examples 1-4 having been received approach, have good coincidence with results from [2].
The all numerical experiments were conducted by computer IBM PC in environment of programming «EUREKA» [5] and have shown the high efficiency of offered approach. By this, the possibility and expediency of unification of calculation problems of strength for reinforced concrete members by reducing them to corresponding problems of NMP. Such approach can be fruitful also for the problems of calculation of strength in which the new physical models of reinforced concrete with plenty of unknown parameters are used and for which the «hand-operated» calculations are highly difficult. The new method of calculation of strength for reinforced concrete structures under the action of cross forces, offered in [6], can serve as example of such problem.

References

[1] SNiP 2.02.01-84. Concrete and reinforced concrete structures [in Russian],TsITP,Moscow,1985.

[2] Aid to the design of concrete and reinforced concrete structures for heavy and light concretes without of prestpressing of reinforcement [in Russian]. TsITP. Moscow,1989.

[3] Himmelblau D. Applied non-linear programming. MIR. Moscow,1975.

[4] Zalesov A.S., Kodish E.N., Lemesh L.L., Nikitin I.K. Calculation of reinforced concrete structures on strength, crack resistance and strains [in Russian]. Stroyisdat. Moscow,1988.

[5] Djakonov V.P. Reference book for application of system «EUREKA» [in Russian]. Nauka Moscow,1993.

[6] Zalesov A.S., Klimov Y.A. Strength of reinforced structures under the action of cross forces.
Budivelnik. Kiev, 1989.

Knowledge-Based System for Dynamic Analysis and Design of Structures

Abbes BERRAIS
Assist. Prof.
Abha College of Technology
Abha, Saudi Arabia

Abbes Berrais, born 1961, received his civil eng. degree form Algeris Univ. in 1985, MCs from Liverpool Univ. in 1988, and PhD from Leeds Univ. in 1992. He is currently an assist. prof. in the construction dept Abha College of Techn., KSA.

Summary

Dynamic analysis techniques for high-rise structures under earthquake effects are rapidly being developed and have been recognized as indispensable tools. The valid use of these techniques requires from the design engineer a comprehensive understanding of the limitations and inaccuracies of the analysis, and constant review of the results for errors. Computer-based structural design assistants are needed to provide engineers with decision support tools and to guide them through the dynamic analysis and design of high-rise structures. Therefore, the incorporation of knowledge-based systems techniques will play a great role in helping carrying out the complicated dynamic analysis and design process. This paper describes the development of a knowledge-based design tool for the dynamic analysis and design of high-rise structures subjected to earthquake forces.

1. Introduction

As structures become more complex in shape, taller and lighter, so the need grows for better and more reliable tools to help in the analysis and design of such structures. Dynamic analysis and design techniques for high-rise structures under earthquake effects are rapidly being developed and have been recognized as indispensable tools. However, their use in design offices requires specially trained and skilled engineers. Understanding the dynamic behavior and ultimate capacity is essential for the design of safe and economical structures. Computer-based structural design assistants are needed to provide practicing engineers with decision support tools and to guide them through the dynamic analysis and design processes. Therefore, the incorporation of knowledge-based systems techniques (KBES) will play a great role in helping carrying out complicated dynamic analysis and design of high-rise structures. This paper is concerned with the following: Development of a knowledge-based design tool (KBDT) for the dynamic analysis and design of high-rise structures subjected to earthquake forces. The design methodology included in this KBDT is based on the *ductility* concept, and is briefly described. Knowledge representation and the coupling of numerical methods with symbolic processing are also considered.

2. Earthquake Design Methodology

In earthquake analysis/design process, the engineer should consider the different factors that control the inelastic behavior of a building. The most critical factors to be considered in earthquake design are *ductility* and the detailing requirements. The earthquake design methodology (EDM) adopted in this research is divided into two phases (see Fig. 1): *preliminary design phase* and *detailed design phase*. In the first phase a simple elastic analysis is employed to establish an initial deployment of reinforcement. In the second an inelastic dynamic analysis is

performed to allow a detailed review and refinement of this reinforcement. The EDM has been applied to a particular type of lateral resisting system, coupled shear wall structures.

2.1 Preliminary Design Phase

This phase comprises three stages (see Fig. 1): conceptual design, preliminary analysis (elastic), and allocate reinforcement: in the *Conceptual design stage*, the overall form of the building is specified together with the relative positions of the lateral load resisting elements. The regularity requirements are checked against codes limitations. In the *Preliminary analysis stage*, an elastic analysis is carried out of the structure under the effect of the lateral static forces obtained in the previous stage. In the *Allocate reinforcement stage*, an initial estimate of elements reinforcement is carried out.

2.2 Detailed Design Phase

This phase comprises three stages (see Fig. 1): *detailed analysis* (inelastic dynamic), *review ductility*, and *refine reinforcement*. In the *Detailed analysis stage*, an inelastic dynamic analysis is carried out by choosing a suitable earthquake record to critically excite the structure. The inelastic dynamic analysis is carried out using the program DRAIN-2D [1]. In the *review ductility satge*, the rotational *ductility* of each structural element is estimated as [2]:

$$\mu_r = \frac{\theta_{\max}}{\theta_y} = \frac{\theta_y + \theta_p}{\theta_y} = 1 + \frac{\theta_p}{\theta_y} \tag{1}$$

Where: μ_r is the rotational ductility; $\theta_{\max}$ is the maximum rotation;
θ_p is the plastic rotation; and θ_y is the yielding rotation

The purpose of the *ductility review stage* is to check the performance of the structure as designed. In the *Refine reinforcement stage*, the reinforcement adopted in the *allocate reinforcement stage* is refined based on the result of the *ductility* requirements in the *review ductility stage*.

3. The Knowledge-Based Design Tool (KBDT)

The aim of the developed KBDT is to assists design engineers in the following tasks:
- Check the regularity requirements of a building.
- Estimate the different earthquake factors used in UBC [3] code requirements.
- Model and perform the inelastic dynamic analysis of the structure under earthquake records.
- Estimate the required reinforcement in structural elements.

A macro level schematic view of the KBDT architecture is shown in Fig. 2. The architecture has the following components:

- *Knowledge base:* comprises of several modules, each module is responsible for a specific task;
- *Context*: contains the collection of facts which represent the current state of the problem in hand;
- *Inference Mechanism*: controls the system by modifying and updating the context using the knowledge in the knowledge base;
- *External analysis programs*: contain the structural analysis program DRAIN-2D, which is interfaced to the system;
- *Explanation facility*: provides the user with the necessary explanations about the task being performed; and
- *User interface*: provides a channel through which the user can interact with the modules of the system.

4. Non-linear Dynamic Analysis Module

The non-linear dynamic module is one of the knowledge-base modules of the system. It is concerned with the inelastic dynamic analysis of RC structures under earthquake records. It uses the DRAIN-2D finite element program [1]. Interfacing with the program DRAIN-2D takes place on three levels:

Input Data Level: At this level data needed for the dynamic analysis is prepared and checked for consistency. The earthquake record is selected from a set of records. The data in the resulting file DRAIN.IN, is read by DRAIN-2D.

Solution Process Level: At this level, the module executes the analysis program DRAIN-2D as a background process. During the inelastic analysis, limited information is displayed on the screen to inform the user of progress. More detailed information is directed to an output file DRAIN.OUT which is investigated at the evaluation level.

Evaluation Level: At this level a quantitative-qualitative transformation of the dynamic analysis results is carried out for the user. The module interfaces to the output file DRAIN.OUT, reads the results it contains, and transforms them into formats and graphical displays suitable for assimilation by the user (see Fig. 3). The results that are displayed and interpreted in this way include the following: Elastic/inelastic lateral deflections; Lateral drift at each floor level; beams moment, axial and shear forces, and bending moments; and rotational ductility.

In case the ductility requirements are not satisfied, or if the walls yield at the base before the beams, the user is informed by the system. The module then assists the user to carry out further inelastic analysis with modified element strength until the design is satisfactory. During the re-analysis phase, the module automatically modifies the input data for DRAIN-2D. The general steps taken to carry out the dynamic inelastic analysis of coupled shear walls are shown in Fig. 4.

5. Knowledge Representation

The knowledge representations used in this system include production rules, frames and data-driven procedures, these being provided by Quintec-Prolog and Quintec-Flex [4,5]. Additionally, the numeric procedures are represented using FORTRAN 77 as external programs. An example of a typical rule that decides on the type of reinforcement configuration to be used in the beams follows:

Rule Beam_reinf1
    IF Vbcr is the critical beam shear stress
    AND min_cal_beam_shear_stress > Vbcr
    THEN compute_diag_steel_area
    BECAUSE
    minum cal_beam_shear stress is > 0.1*beam_length*fcu**0.5/beam_height

An example of using Quintec-Flex frames is the representation of earthquake records for use by the program DRAIN-2D. The San Francisco record is represented as frame with slot values as shown in Fig. 5.

6. The User Interface

The acceptability of any KBDT depends largely on its user interface. The design of a good user interface must consider many aspects of human computer usage ranging from cognitive models of the user's thought processes to the aspect of usability. It is assumed that the user is knowledgeable

about structural design, but not necessarily about dynamic analysis concept. The following system requirements were identified and form the objective of the system implementation:
Easy to use; Takes the initiative and question the user; Teaches the user how to formulate the problem; Allows the user to invoke the system at any level of abstract; and informs the user about the next step in the design process. The user interface of KBDT is shown in Fig. 3.

7. Conclusions

In this paper a prototype KBDT for the dynamic analysis and design of high-rise structures was described. The prototype system helped on the iterative design to achieve a balance between element strength and stiffness to fulfil ductility requirements. The integration of symbolic processing and dynamic analysis methods is a necessity for a robust and practical computer-aided earthquake design. Moreover, KBES technology could be used in collecting and managing earthquake engineering expertise from different sources and formalizing this knowledge for future use by less experienced engineers. Heuristics alone are not sufficient to solve real design problems. The system needs to be linked to numerical and structural analysis modules.

The KBDT has accomplished the following:

- Automate much of the dynamic analysis/design process, which could free the design engineer from the more tedious aspects of design and allow him to concentrate on concepts such as ductility.
- Help the structural engineer on the efficient use of FEM programs, preparation of input data, modeling, and interpretation of results.
- Minimize the time spent to prepare the input data to the program DRAIN-2D, and help the structural engineer in the decision making process.
- Enable the designer to control the location and magnitude of inelasticity in structural members using inelastic dynamic methods. This allows the engineer to design the structure based on the ductility concept.

References

1. Kannan, A. E., and Powell, G. M. (1975), "DRAIN-2D, a general purpose computer program for dynamic analysis of inelastic plane structures", Rep. No. EERC 73-22, Earthquake Engineering Research Center, University of California, Berkley, USA.
2. Fintel, M., and Ghosh, S. K. (1982). Explicit inelastic dynamic design procedure for aseismic structures, ACI Journal 79, pp. 110-119.
3. ICBO 1991 UBC:91, *Uniform Building Code*, International Conference of Building Officials, Whittier, CA.
4. Quintec System Ltd. (1989). *QUINTEC-PROLOG*, System Predicates, Unix version, UK.
5. Quintec System Ltd. (1989). *QUINTEC-FLEX*, User Manual, Unix version, UK.

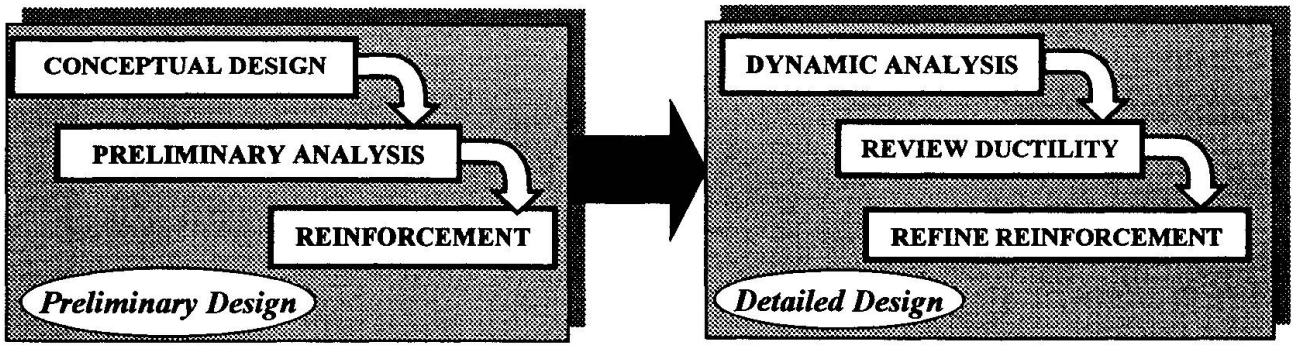

Fig. 1 Earthquake design methodology

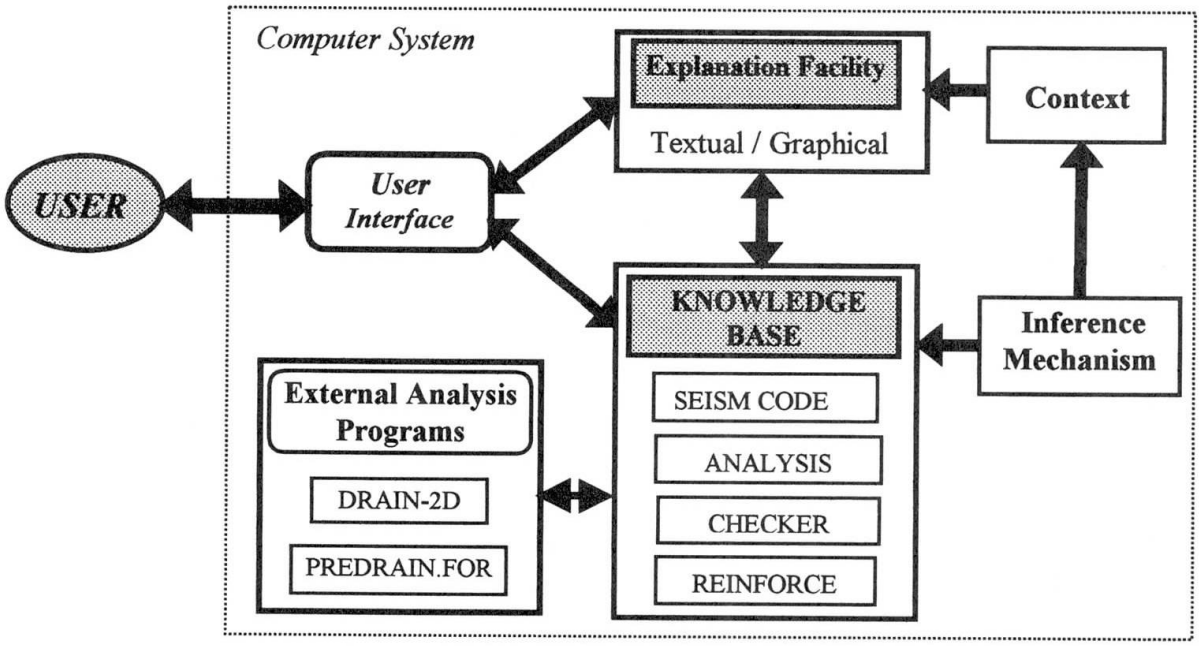

Fig. 2. Architecture of the KBDT system

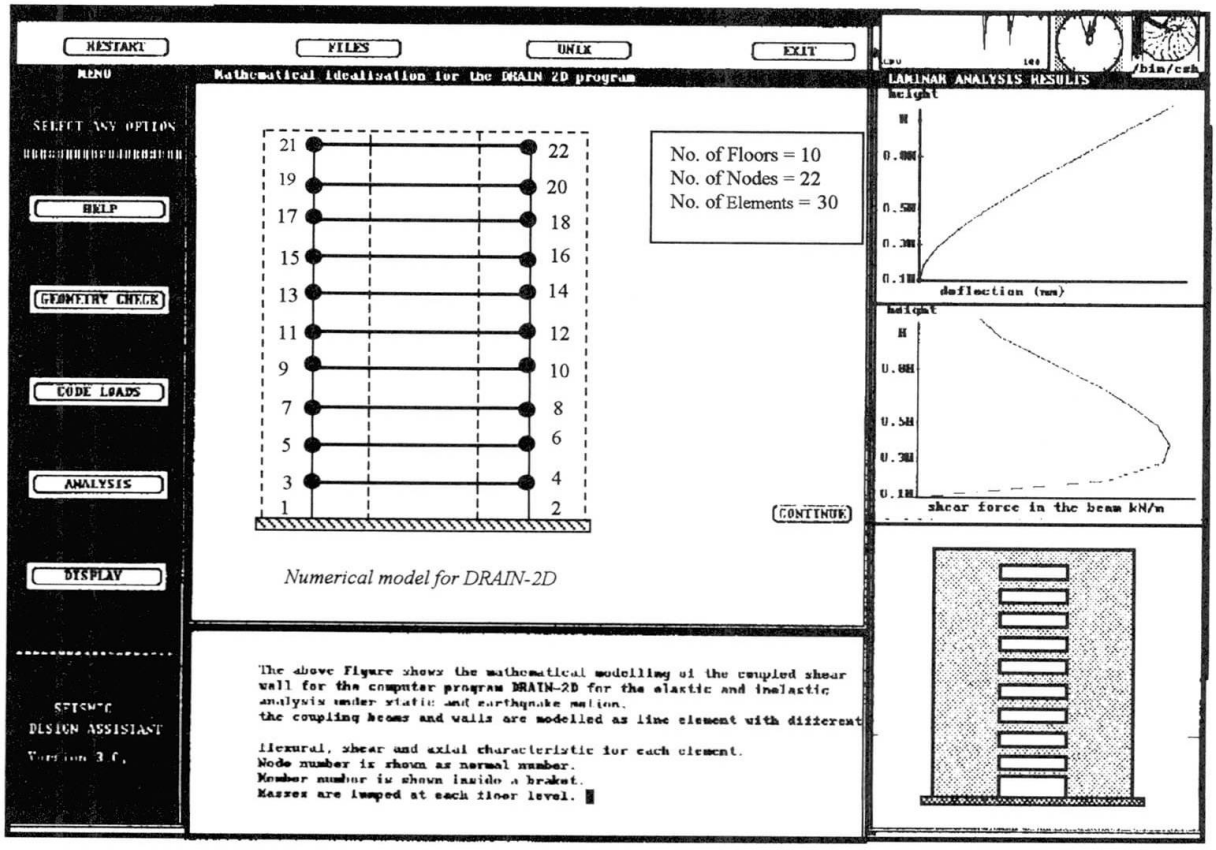

Fig. 3. User interface of the KBDT

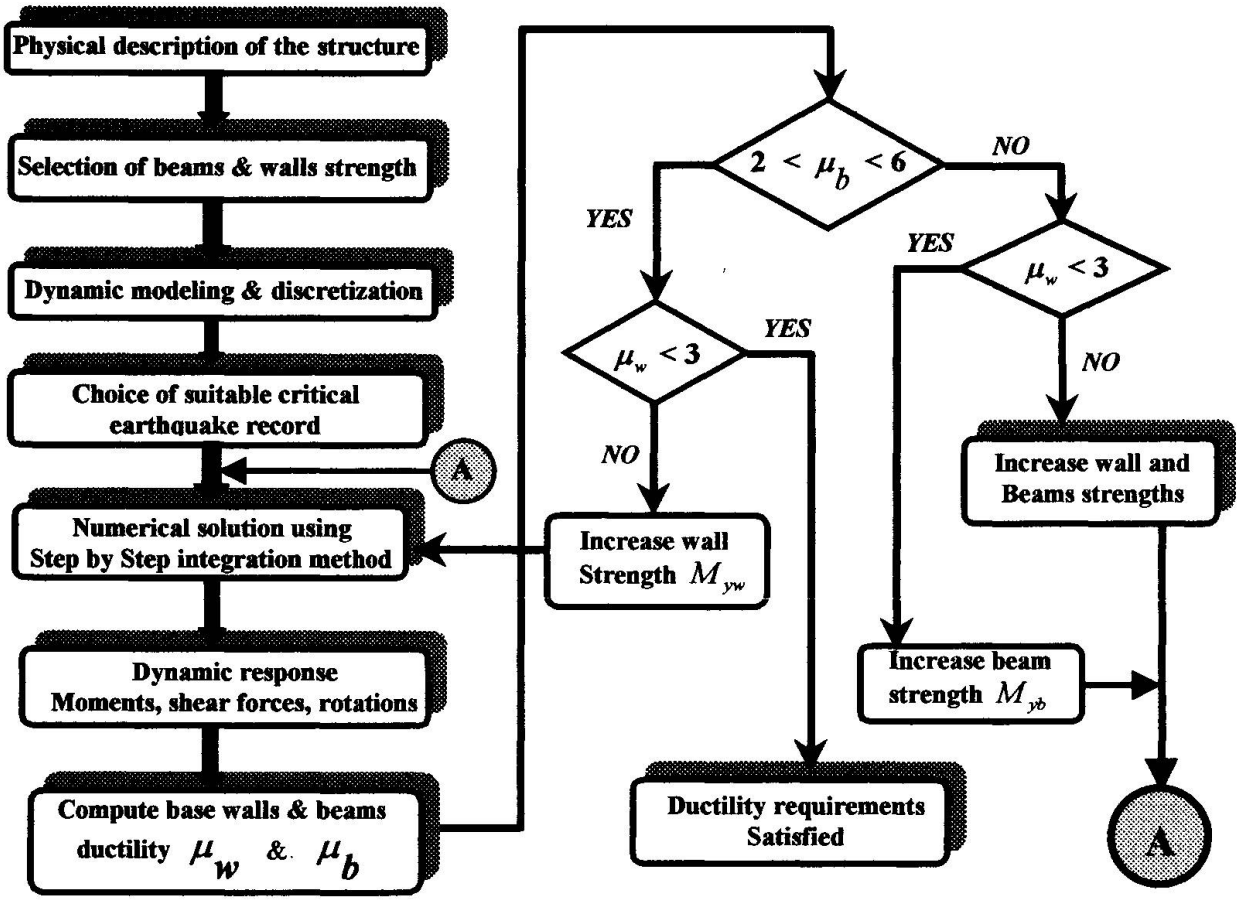

Fig. 4. Flowchart for dynamic inelastic analysis procedure

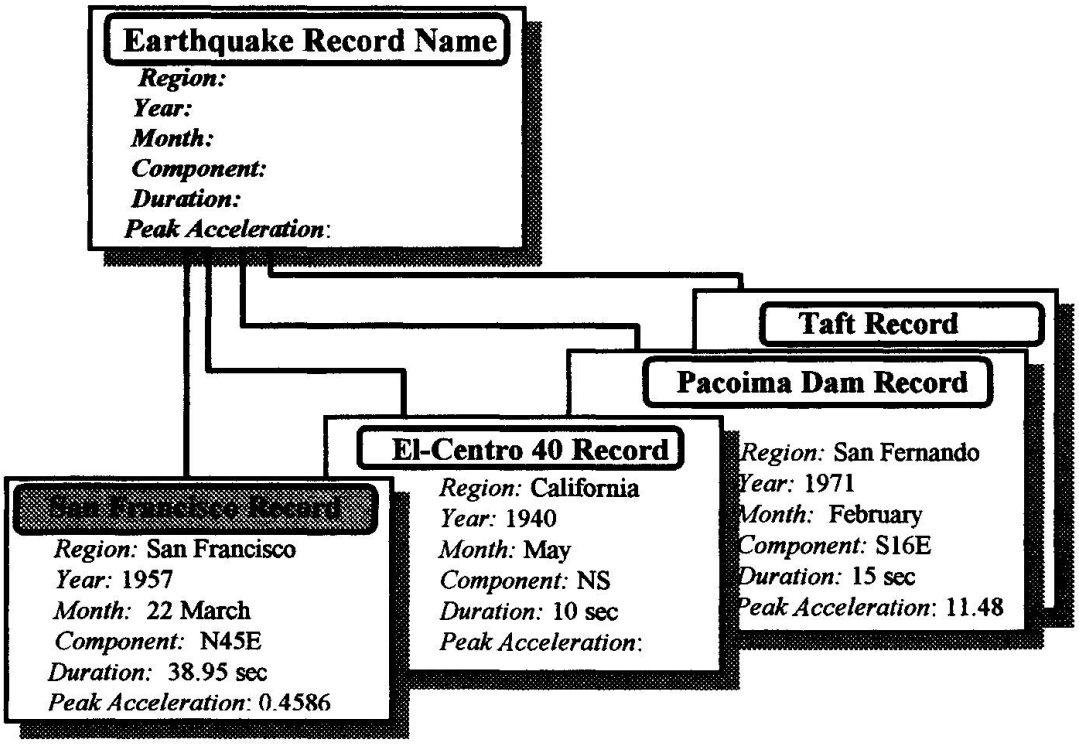

Fig. 5. Frame representation of different earthquake records

Monitoring the Big Bridges across the Danube in Austria

Helmut WENZEL
Dr Eng.
Vienna Consulting Eng.
Vienna, Austria

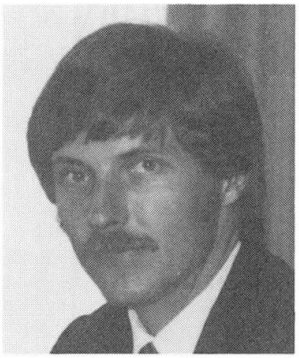

Helmut Wenzel is a member of WC V of IABSE. He earned a Ph.D. in Bridge Constr. from the Univ. of Vienna in 1978 and is the Managing Dir. of VCE, with offices in Vienna, Taiwan and Korea. Dr Wenzel also teaches Bridge Design and Construction at the Univ. of Vienna.

Summary

Since the spectacular collapse of the famous Reichsbrücke in Vienna in the year 1976, the attention of Austria Bridge Engineers is very much focused on the big bridges across the Danube. The frequency of traffic on most of the bridges has reached the limit, touching some 140.000 vehicles per day in the extreme cases. This vital lifelines have to stay open under any conditions. Therefore the assessment of the structural condition of the bridges is of upmost importance. This paper reports on the works carried out on the bridge assessment covering 9 major bridges with the use of the dynamic characteristic method BRIMOS developed by VCE. The potential of the method is demonstrated and relevant tests are provided.

1. Introduction

The main target of the works was to create a numerical tool for the assessment of the structural stability of the major bridges across the Danube. As a basis the tools of the vibration characteristic method was used. It is based on Ambient Vibration Tests carried out on the bridges frequently. They are compared to analytical calculations with Finite Element computer models, which represent the planned condition of the structure.

The Bridge Monitoring System BRIMOS has been developed over the past 2 years to carry out ambient vibration tests economically. Useful results for the assessment are provided. The major mile stones of the program are:

- Recording of the characteristic through 8 accelerometers which are moved over the bridge to cover the whole area
- Calculation of a representative spectrum, which represents the dynamic characteristic
- Calculation of structural damping by filtering out certain Eigenfrequencies and extraction of damping with the use of the Random Decrement Technology (RDT)
- Numerical assessment on structural integrity under consideration of the measured values
- Determination of the Eigenform as a confirmation for the fitting of calculation and measurement
- Search for damage indicators in the signals and location of the damages

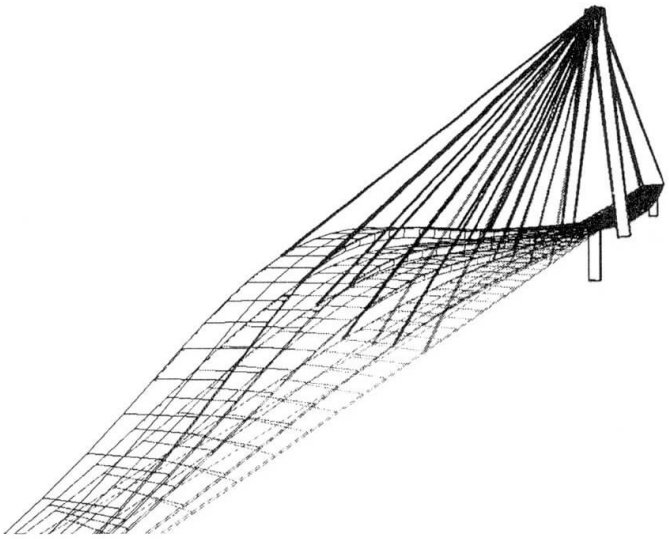

Fig. 1 Eigenmode animated from measurement

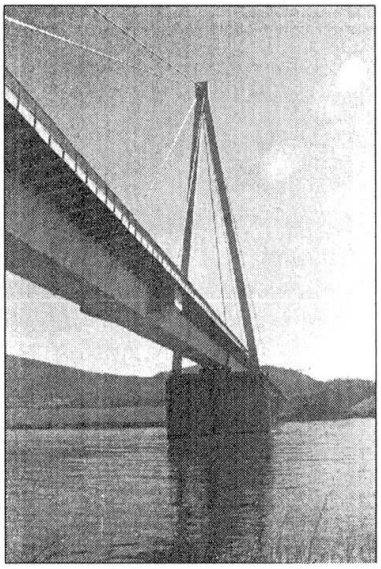

Photo 1 Hainburg bridge

For each structure a report is prepared providing the basic dynamic characteristic, an assessment of structural safety, the values of damping for the structure and the assessment of eventual hidden damages. In the long-term it is intended to undertake measurement frequently and to calculate trends from the results.

The method has been proven by a number of tests in the laboratory and by a major number of tests on bridges on site.

2. The Bridges across the Danube

In Fig. 6 of this paper the bridges considered in this report are described. All kind of structures are represented. There is a number of cable stayed bridges made from steel or concrete or even composite deck structures, a number of steel bridges with various spans, a major composite bridge and a long span concrete bridge. Due to the huge amount of structures and data only representative results can be provided.

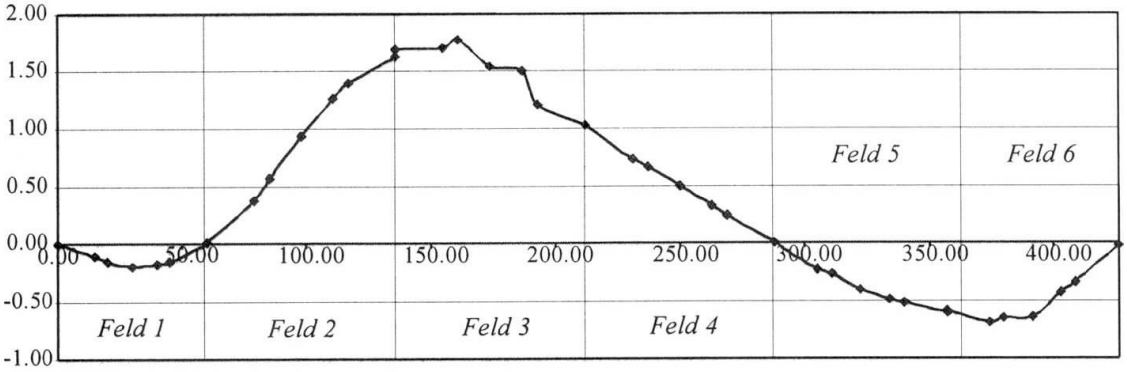

Fig. 2 1. Vertical Eigenmode of the Hainburg bridge

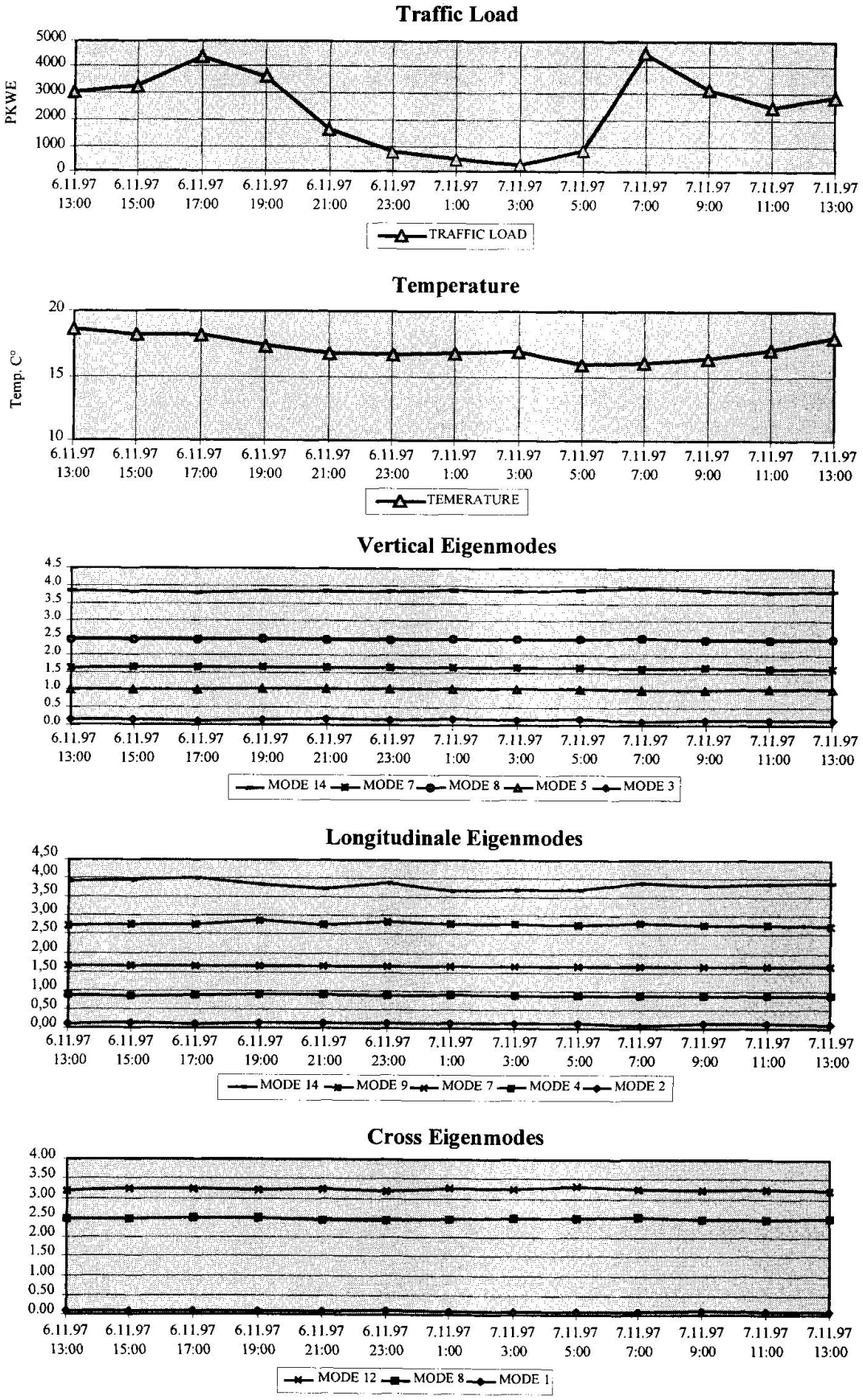

Fig. 3 24 hour test results, traffic load, temperature, frequencies

3. Tests and Calculations

For each of the structures a base measurement has been established. It consist of a minimum of 5 measurement points per span and side of each deck structure. The time requirement for a serious test of a bridge of 200 meter length is approximately 10 hours. The characteristic is recorded at a Sampling – Rate of 100 Hertz and per measurement 50.000 points are stored. Amplifiers and filters are used according to the requirement of each structure. The system is calibrated by a laser displacement device, which provides actual displacement in millimeters. For each of the bridges a dynamic Finite Element Calculation is carried out. It concentrates on the idea of the designers and follows strictly the drawings. Therefore it will be representative for the "should be" case. It serves to define the starting point of the life time performance check.

4. Major Results

The Eigenfrequency of a structure is depending on a couple of items out of which the most important are: The mass, the stiffness, super imposed dead loads, traffic loading both static and dynamic, strain from temperature difference, internal stresses from prestressing and some minor other phenomena not yet fully understood. The method had to be calibrated against those influences to focus the results on the most useful influences, which are stiffness and damping.

One of the most important items was to demonstrate, that the ambient vibration method produces reliable results independent from the traffic loads applied. This was done by means of a 24^h test on one of the representative bridges, which is the Nordbrücke. Permanent measurement has been carried out on a day, where the change in air temperature was only 2°C. The traffic on the bridge varied from 130 vehicles at 3 o'clock in the night to almost 5.000 vehicles per hour during the peak traffic at 7 o'clock in the morning. The variation in the results, considering more than ten fundamental modes is in average below 1 %. This means, that ambient vibration data can be extracted almost under any traffic conditions. The enclosed Fig. 3 show the results over 24 hours including the temperature change, the vehicle loading and some of the relevant eigenfrequencies.

Bridge	1. Vertical	Damping	max. span	Deck
Hainburg	0.53	1.12%	228.00	steel
Donaustadt	0.67	0.44%	1.86.00	composite
Reichsbrücke	0.83	0.68%	170.00	concrete
Brigittenau	0.75	1.67%	175.00	steel
Floridsdorf	0.77	1.44%	167.50	steel
Nordbrücke	0.86	2.30%	83.40	composite
Tulln	0.53	1.60%	176.00	concrete
Melk	0.70	1.64%	190.00	concrete
Steyregg	1.23	1.63%	181.00	composite

Tab. 1 Vertical frequency and corresponding damping

Another major task was to perform the identification of the Eigenmodes from the measured data. This is demonstrated at the Hainburg Cable Stayed Bridge. The Fig. 1 and 2 show the calculated Eigenmode as well as the measured one. It is obvious that the results are very good. The measured modes are carried on to an animation program, which produces real time or accelerated demonstrations of that measurement. These are compared with the calculations and the differences are identified. Very often the interpretation is simple. It gives an idea about the

function of important parts of the structure. Both, calculation and measurement, can be superimposed to demonstrate the differences.

5. Damage Identification

The identification of damages beyond the results of visual inspection are the development area of the future. It is well established, that any damage is represented in the signals. The difficulty hides in the interpretation. It was observed, that the results are varying very much depending on the qualification of the operator. Very good results have been achieved by bridge engineers, which learned to handle a monitoring system. Monitoring engineers normally failed to assess abnormal recordings, which they tended to identify as problems with the monitoring system.

Therefore the main task shall be to identify patterns of signals, which indicate a normal condition. A typical example is shown in Fig. 5, which represents a crack in a prestressed concrete structure. The so called double peak in the 1. vertical Eigenfrequency, effected are mainly the lower frequencies, indicates a variation of stiffness with a variation of amplitude, i.e. traffic loading. In this case the evaluation of periods with passenger car loading provides the lower frequencies as the case with truck loading. This indicates, that the crack is open under normal conditions and closes when trucks excite this structure. Feeding this information into the finite element model it can be calculated that a crack, reaching from the bottom of the structure 60 cm into it, is active. The location of the crack was also determined, to be a construction joint. This theory has been confirmed through measurement on other structures, with well known active cracks.

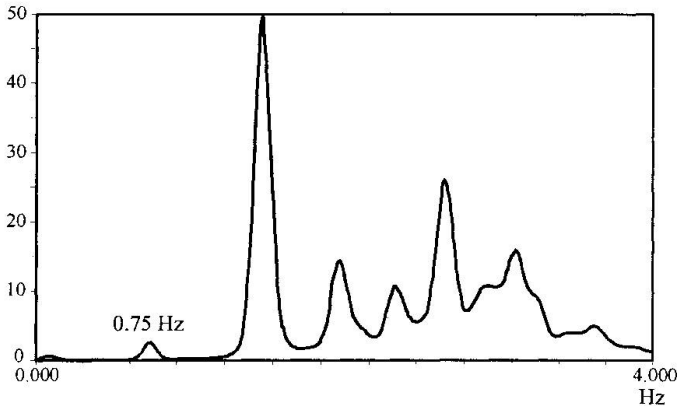

Fig. 4 ANPSD of Brigittenau

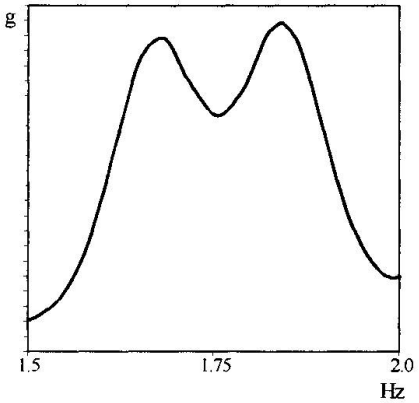

Fig. 5 Double peak

6. Conclusion

The promising results of the ambient vibration tests make it necessary to invest in further development of the damage identification tools. It will not be possible to find easy and closed solutions for most of the problems. Therefore an identification routine based on Fuzzy Logic will be necessary. It has been started already to collect relevant results of bridges as many as possible. These will be stored in a data bank, which will form the basis for comparison of cases. Although it is clear, that it will still take a long time to make these methods simple, the proof has been provided, that it works. A key issue of the subject is the education of bridge engineers in dynamics and monitoring to provide the basis for the understanding of the procedures and physics. For this purpose more major demonstration projects shall be implemented.

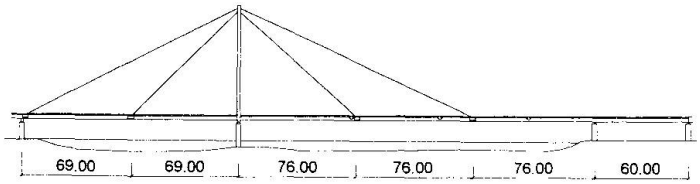

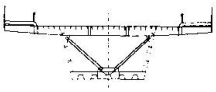

Donaubrücke Hainburg

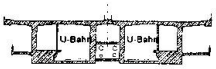

Reichsbrücke

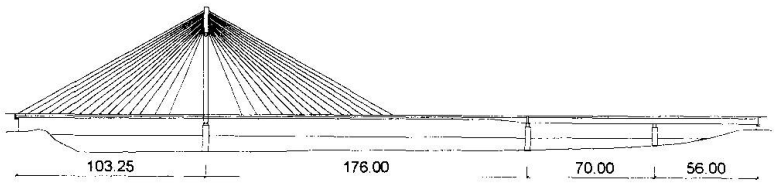

Tulln West Bridge

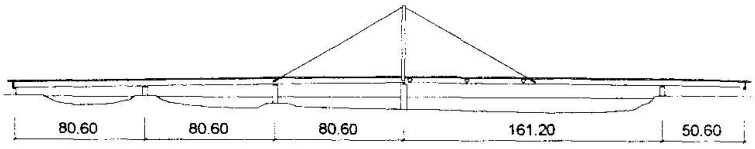

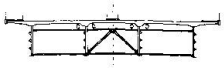

Donaubrücke Steyregg

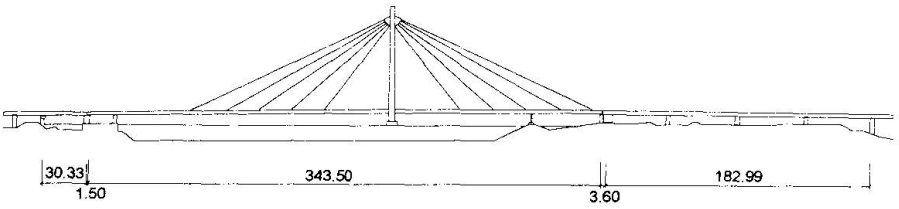

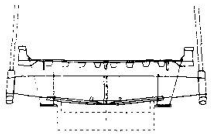

Donaustadtbrücke

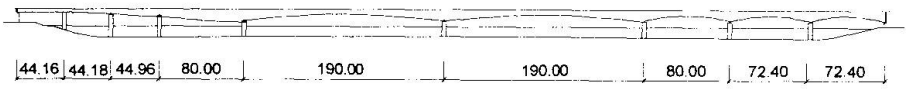

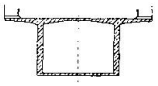

Donaubrücke Melk

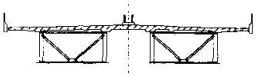

Nordbrücke

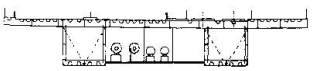

Donaubrücke Floridsdorf

Fig. 6 Bridge dimensions

Dynamic Tests and Monitoring of a Highway Bridge over the Danube

Jan BENCAT
Prof.
Univ. of Zilina
Zilina, Slovak Republic

Jan Bencat, born 1943, received his eng. degree in 1967 form TU Cracovia (Poland) and Ph.D. at UTC Zilina in 1973. He is currently Prof. of Structural Mechanics at Civil Eng. Faculty, Univ. of Zilina.

Summary

The dynamic response behaviour of a prestressed concrete seven span highway bridge (761,0 m long) was examined in September 1990 as a part of the static and dynamic loading tests (DLT)of the bridge. In this investigation, a structural measuring technique using vehicle-induced vibrations as well as forced vibrations induced by the rocket engines was developed for fullscale testing of the bridges. The data yielded the dynamic characteristics of the bridge e. g. natural frequencies f(j), mode shapes, dynamic load factor δ (DLF) and the damping of the structure (ϑ). The obtained dynamic characteristics were compared with the theoretical computed data. Monitoring of the highway bridge over the Danube (La Franconi Bridge) has been carried out in 1991-1997, to evaluate the accuracy when using a simple measurement of a well defined eigenfrequency to give a long term overall indication of deterioration or crack formation.

1. The Bridge Arrangement and Dynamic Loading Test

The main bridge structure is composed of seven span continuous beams with one frame pier (P3). Other supports are formed by seven massive piers. The total length of the bridge is 761.0 m with spans 83.0 m + 174.0 m + 172.0 m + 4 x 83.0 m. The highway bridge consists of two independent bridges (left and right bridge -LB,RB) with three traffic lanes, on each bridge for one direction only and sidewalks on both sides. The bridge box cross-section is shown in Fig. 1 and the longitudinal section, in Fig. 2. The bridge including multispan junctions is fully described in [1].
*Testing procedure and experimental analysis.*The test programme included field measurements using the instrumentation described in [3] so as to ensure coverage of entire possible range of vibration. The vibration amplitudes were investigated and recorded in 18 selected points. The time history of vertical as well as horizontal vibration has been registered by accelerometers (Brüel-Kjaer, BK-8306) in the 2nd and the 3rd span of the bridge (A1-A8) and in the other spans by inductive displacement transducers (IDT, range ±40 mm), points R1- R10, see Fig.1 and Fig.2. Output signals from the accelerometers were preamplified and recorded on two four-channel portable tape FM recorder (BK-7005) and simultaneously via DISYS software on PC/486 at the measuring station DMS-1. The signals from the IDT were recorded simultaneously at the station DSM-2 and DSM-3 by the same way as the signal from accelerometers. The experimental analysis has been carried out in the laboratory of the Department of Structural Mechanics UTC Žilina.

The dynamic load factor δ_{OBS} and frequency response spectrum (PSD) has been determined using the record obtained from passing vehicle velocities over the bridge by computer PC/486 via DISYS programme and two-channel real time analyzer BK-2032. *Testing load and experimental results.* The use of the test load has been in accordance with [3]. Two lorries TATRA-815 of mass 26 660 kg and 26 740 kg were used for the highway pavement. Rocket engines (RE) impulsive load were separately used, too. Static loading test (SLT) was perfomed before the

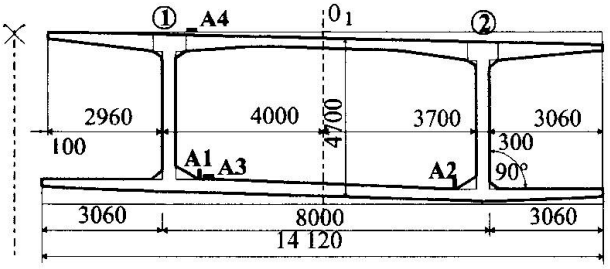

Fig.1 Bridge cross section

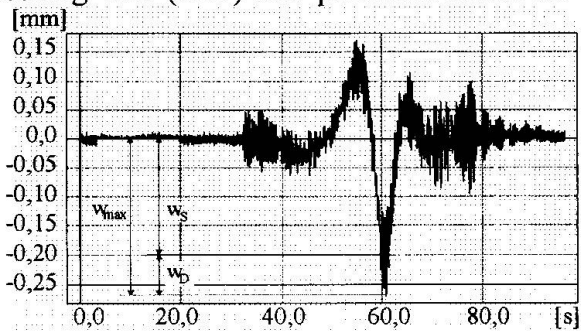

Fig.3 Time history of bridge vibration due to passing vehicle at the point 117(v –62,91km/h)

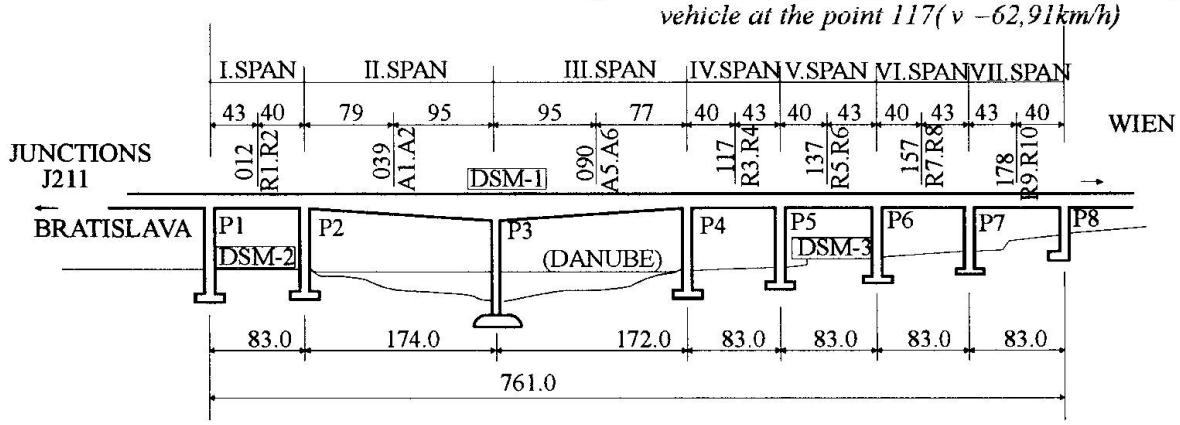

R1...R10 - Transducer Positions, A1...A6 - Accelerometer Positions

Fig.2 Longitudinal section of the bridge

dynamic loading test (DLT) with both vehicles TATRA-815. Experimental procedures have been discussed in detail by autor [3]. Formula (1) gives the criteria [2] for evaluation of moving load dynamic effects on the bridge structure

$$(\delta_{OBS} - 1)\eta_{DYN} \leq (\delta - 1) \qquad (1)$$

where (see also Fig. 3), $\delta_{OBS} = w_{MAX} / w_S$ and $\eta_{DYN} = w_{DYN} / w$ The vertical static displacements at characteristic joint (012-178) due to standard live load (w) and due to testing load (w_{DYN}) have been computed by the bridge designer [1]. The calculated dynamic effectiveness η_{DYN} with theoretical and experimental values of the vertical displacements varied in the range η_{DYN} =0,09 ÷ 0,154, for different span of the bridge. The dynamic load factor δ (DLF) used by the designer for the bridge under investigation according to [4] is δ = 1.10, see also [1]. DLF of the experimental tests [3] are obtained from formula $\delta_{EXP} = 1 + (\delta_{OBS} - 1)\eta_{DYN}$, see also Fig. 3. The DLF against vehicle velocity are plotted in Fig. 4, 5. Natural frequencies have been obtained by using the spectral analysis from recorded responses due to various types of dynamic loading, see also Table 1. Since the accelerometers recorded only the dynamic component of vibrating structures, so we can consider those signals as an ergodic and stationary. The results of the analysis are fully described in [3]. Only two PSD are shown in Fig. 6, 7 of this paper. The comparison of theoretical (FEM) and experimental results of the natural frequencies *f(j)* of the vibration bridge according to [3] are presented in Table 1.

The spectral analysis of the vibration time histories made it possible to ascertain the dominating frequencies of bridge vibration by sharp peaks plotted in power spectra. The character of the vibration caused is heavily dependent on dynamic response excitation.

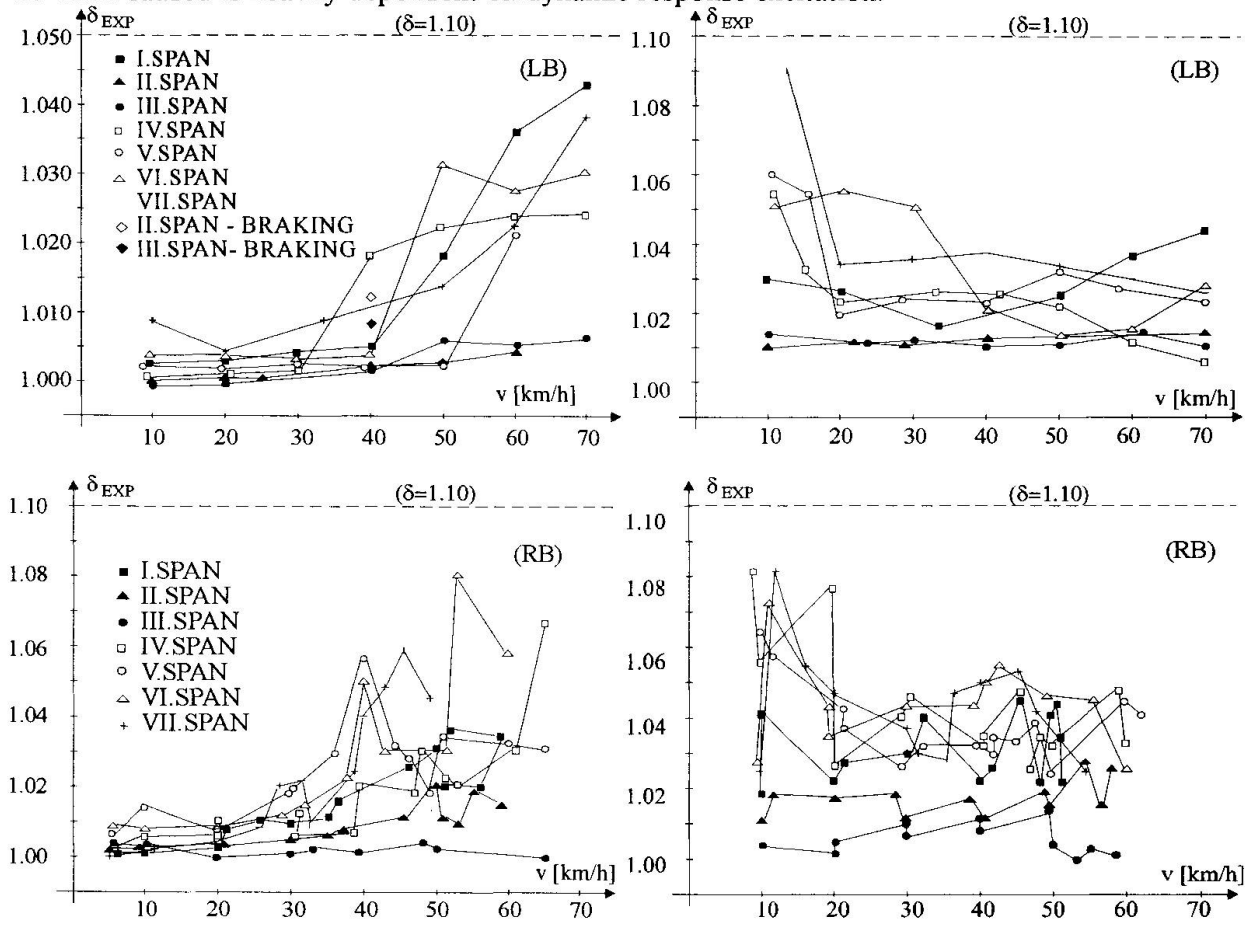

Fig. 4 DLF δ_{EXP} against vehicle velocity - vehicle smooth passing

Fig. 5 DLF δ_{EXP} against vehicle velocity - vehicle obstacle passing

The results of the correlation analysis [3] showed that the vibration of the bridge is not ambient vibration. The bridge vibration has predominate vertical components (bending vibration). In this tests it was possible to predict the damping characteristics according to [2] by using logarithmic decrement.The evaluation of the logarithmic decrement ϑ has been done from records of fre bridge vibration due to impulse rocket engines. The logarithmic decrement corresponding to the first and second modes of the bridge vibrations varies in range ϑ=0,024 ÷ 0,049.

3.Bridge Dynamic Parameters Monitoring

Progressive deterioration of concrete structures (RC) due to alkali silica reactions and frost-thaw influence has become a serious problem. It has increased the importance of making observation on full scalle structures in order to obtain the experimental results necessary for the development of theories for predicting service life.

It has been the scope of this work to evaluate whether the relative change of a well defined natural frequencie or the change of the corresponding damping and the change of RMS value of the displacements amplitude of the bridge vibration observed by traffic loading can be used to give an overall indication of deterioration or crack formation. The monitoring technique based on

measurement of the time history of the bridge vibration due to regular traffic is not meant to give detailed information but to be a technique simple to use to deside whether more detailed methods should be used.

During the years 1991-1997 La Franconi bridge over the Danube has been investigated by 24 hours monitoring tests in the summer and the winter time . A theoretical prediction of the bridge behaviour and preliminary dynamic loading tests are reported in [3].

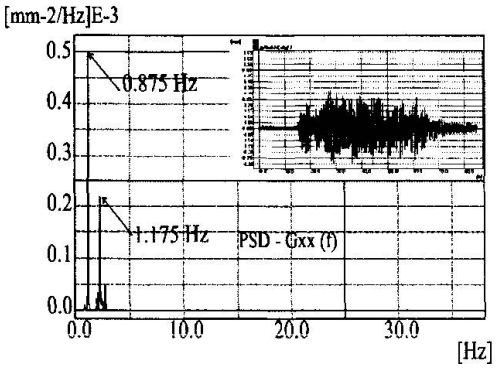

Fig.6 PSD at point 039 caused by TATRA 815

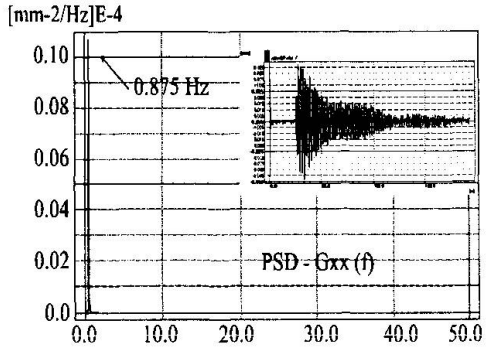

Fig.7 PSD at point 039 caused by RE

NATURAL FREQUENCIES / Hz /			EXCITATION TYPE
f(j)	CALCULATED	MEASURED	
1	0,865	0,875	RE, TATRA 815 - BR
2	1,157	1,175	TATRA 815 - OBST
3	1,919	1,9	RE
4	2,042	2,148	TATRA 815
5	2,3	2,275	RE, TATRA 815 - OBST
6	2,686	2,775	RE, TATRA 815 - BR

Table 1 The natural frequencies

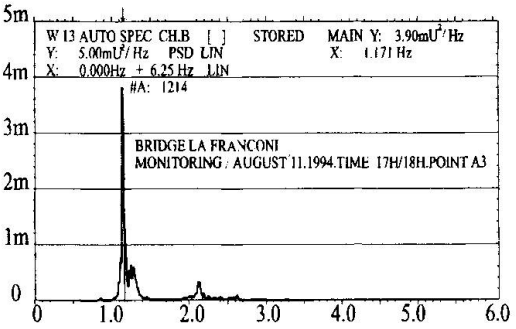

Fig. 8 Monitoring PSD at point 039

Testing procedure and experimental analysis. The vibration amplitudes were investigated and recorded in selected points of the second and the third span, see Fig. 1, 2. The time history of vertical vibration has been registered by accelerometers (Brüel-Kjaer, BK-8306) at points 039 and 090 (A1, A2, A5, A6) on each independent bridge.

Output signals from accelerometers were preamplified and recorded on four-channel analogue FM recorder BK-7005 and simultaneously via A/D convertor DAS-16 on portable notebook computer (PC/486) with special software (DISYS) and hardware facilities for 24 hours continuing test. The records obtained in the bridge monitoring tests were investigated by using frequency analyser BK-2034 and mentioned PC facilities. Fig. 8 shows power spectral densities (PSD) as an example of the spectral analysis of the monitoring test performed in August, 1994. The damping parameter (D-critical damping coefficient) was found by means of the 3dB bandwith method and curve fitting techniques. The amplitude analysis has been used to obtain RMS amplitude value of the bridge vibrations during the monitoring tests.

Experimental results. Results giving frequency and damping for lovest natural frequency in bending and RMS amplitude value from the monitoring tests of the bridges during whole measuring period are shown in Fig. 9. A 2.7% change in frequency is observed during a year (summer-winter) but it is systematic from one year to the next and is partly due to changes in ambient temperature. By measuring the frequency at the same time of year the changes from year to year are small and non systematic and correspond to a coefficient of variation of about 0.01. This may be considered negligible compared with the changes in natural frequency of about 30% corresponding to advanced deterioration observed in [5].

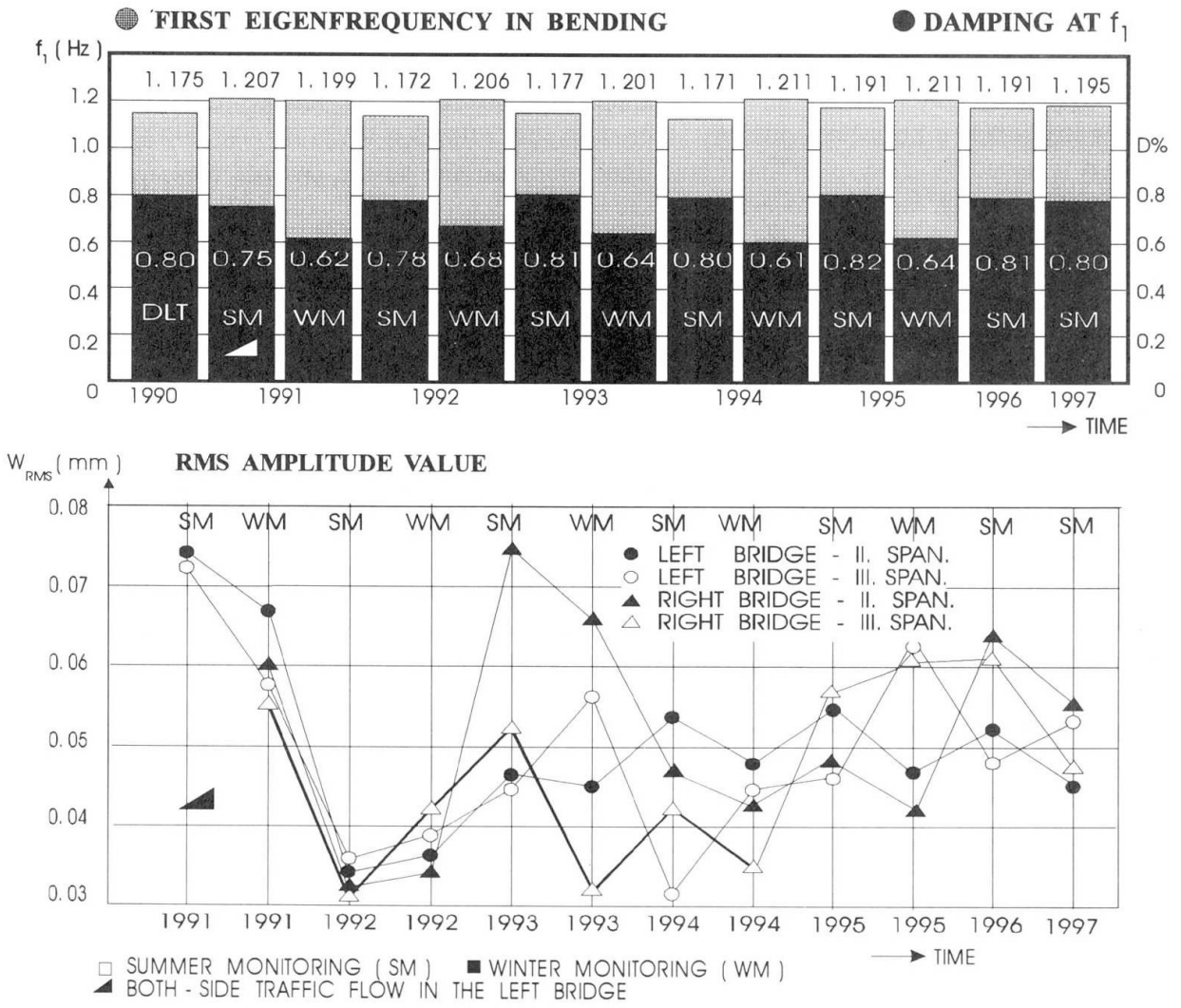

Fig.9 Changes in relative frequency, damping and displacement RMS amplitude values, 1990 - 1997

There is not the same systematic change of damping and scattering of results is big. What causes these changes is not clarified. There are changes in the temperature during the day. This may give changes in length of bridge which can influence support conditions and damping. Windspeed, water level, ambient relative humidity and temperature gradients through the deck, transport in the bridge deck, in particular at the surface, and may there by also change damping [6],[7].

There is a difference of the discplacement amplitude RMS value measured in may 1991 in comparison with other measurements results. It was maybe caused by both-side motor traffic flows on the left bridge. All the following measurements were performed in conditions of the one side traffic flow on each of the two bridges La Franconi. The changes of the amplitude RMS value is caused mainly by changes of the intensity of the regular motor traffic.

4. Conclusion

The experimental analysis of the bridge dynamic response caused by moving load as well as impulsive load made it possible to identify six basic modes of bridge vibration. These frequencies have been received by analysis of small amplitude vibration and so the analysis corresponds to linear vibration. It was possible to evaluated the damping characteristics of the bridge structure only from limited number of measurements. They are therefore only indicative. The experimentally achieved dynamic load factor $\delta_{EXP}<1,09$ shows that real stiffness of structure is fully comparable with the corresponding value for, $\delta = 1,10$ obtained by computation. The comparison of theoretical and experimental results of the bridge parameters shows good agreement of theoretical and experimental values of natural frequencies. The criteria of all loading states by the Slovak standard [2] are seen to have been fulfilled.

The monitoring tests results show that the relative change of a well defined natural frequency seems to be very little influenced by changes in temperature, humidity, support conditions, etc., in fully hardened not deteriorated RC structure of simple geometry, if measurements to be compared are made at the same time of the year. This indicates that the monitoring tests may prove useful by giving an idea of the overall development of long term deterioration and cracking in RC structures. The change in structural damping can so far not be used in a similar way because of its big dependance on mentioned secondary influences which are comparable with deterioration or cracking influences on change of structural damping.

The changes in deflection amplitude RMS value are heavily dependent on intensity of regular motor traffic in the bridge deck, but vary within of the 50% RMS amplitude range measured during the whole measuring period.

5. Acknowledgment

The research was supported by the Ministry of Education and Science of Slovak Republic via Scientific Grant Agency - VEGA and Highway Directorate Bratislava which has given free acces to the bridge described in the paper. This support and assistance is gratefully acknowledged.

References

[1] ŠEVČÍK, J. et. al. (1989): "The Highway Bridge D-201-HMO over the Danube in Bratislava". Static Computations Research Report, Dopravoprojekt Bratislava, (in Slovak)

[2] The Slovak Standard No. 73 6209 - Loading Test of Bridge

[3] BENČAT, J. (1990): "Report on Dynamic Loading Test Results of the Highway Bridge D-201-HMO over the Danube in Bratislava ".Report HZ-1-102-90/2.UTC Žilina ,Dept.of Structural Mechanics, (in Slovak)

[4] The Slovak Standard No. 73 6203 - Bridge Loading

[5] Askegaard, V. & Lanso, H. E. (1986): "Correlation between Changes in Dynamic Properties and Remaining Carrying Capacity", Materiaux et Constructions, Vol. 19, No. 109, 11-20

[6] Swamy, N. & Rigby, G. (1971): "Dynamic Properties of Hardened Paste, Mortal and Concrete". Materiaux et Constructions, Vol. 4, No. 19, 13-40

[7] Casas, J. R. & Aparicio, A. C. (1994): "Structural Damage Identification from Dynamic-test Data". Journ. of Struct. Eng., Vol. 120, No. 8, Paper No. 3439

Reconstruction Design for PC Girders Damaged by the Kobe Earthquake

Hidesada KANAJI
Civil Eng.
Hanshin Expressway Public Corp.
Osaka, Japan

Hidesada Kanaji, born 1962, received his Master Degree of Eng. in 1988 from Kobe Univ. He has been engaged mainly in designing expressway structures and supervising construction site.

Summary

The bridge discussed in this paper has simple composite PC girders supported by six RC T-beam piers and one RC rigid frame pier. It is located in Nada Ward, Kobe and was severely damaged by the Kobe Earthquake. The damage included inclination of the eccentric piers and damage to the end cross beams. To restore the bridge, a girder connection with isolators was used to distribute and reduce inertia force. Specifically, the slab-rubber-hinge girder connection method was developed. Isolators with both lead-rubber bearings (LRB) and sliding rubber bearings (SRB) and restrainers having rubber-sheathed chains were also used. Foundations, piers and girders except the damaged end cross beams were reused with some repair.

1. Basic of Structural Framework Design

In the design, focus was placed on developing a girder connection structure and employing omnidirectional seismic isolation to decrease both longtudinal and lateral inertia forces acting on eccentric piers whose reinforcement possibilities were limited (see **Fig. 1**). The preliminary design was first drawn up by applying the seismic coefficient method and the final, comprehensive design was based on the nonlinear dynamic analysis of the seismic record of the Kobe Earthquake at the Japan Meteorological Agency Kobe station. In addition, to verify the validity of the adopted isolated structures, the cumulative strain energy was calculated by analysis of the entire bridge, obtaining the proportions of seismic energy shared by the foundations, piers and isolation bearings (see **Fig. 2**).

2. Characteristic Structure Components

2.1 LRB-SRB Combined Isolation System

Two kinds of bearings, shown in **Fig. 3**, were applied to the bridge. SRBs were placed under the main girders to support the vertical load, and LRBs were placed in the gaps left under the end cross beams by removing part of their underside to absorb inertia force during an earthquake. This system was applied to the bridge in this paper which made use of thin rubber pad bearings

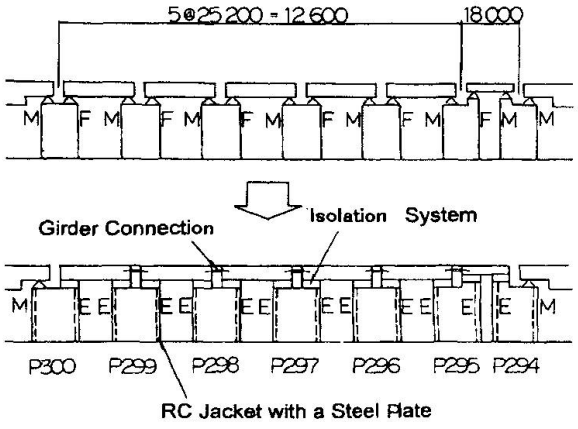

Fig. 1 Structural Framework

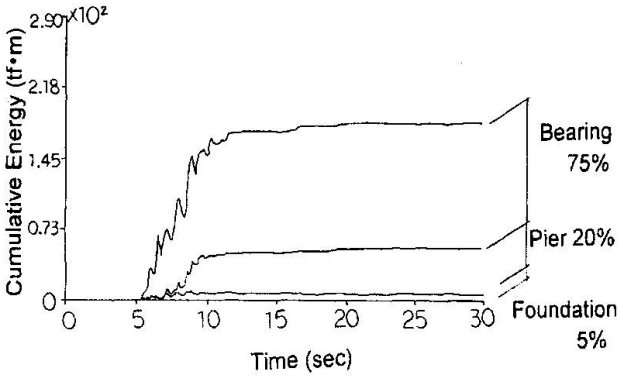

Fig. 2 Cumulative Strain Energy

under girders so as to limit the vertical change in that part of the bridge. The following are the main results verified by the performance tests: (1) the horizontal stiffness and damping capacity of LRB depended on the vertical load, but were within the design limit regardless of the small vertical load; (2) there were no significant changes in horizontal stiffness or damping capacity, regardless of the direction of vibration; and (3) the friction coefficient of SRB was approximately 0.1.

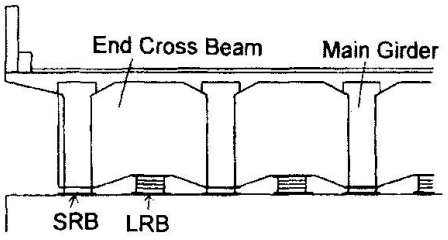

Fig. 3 LRB-SRB Isolation System

2.2 Connected Girder Structure

The girder connecting sections were designed to satisfy the following conditions: (1) the rotation of the joint section due to live load deflection would not be restricted; and (2) inertia force in the longitudinal direction would be transmitted through the joints. Accordingly, new slab-rubber-hinge designs as shown in **Fig. 4** were adopted. In this method, a rubber functioning like a hinge was placed on the slab and the upper parts of the cross beams were connected by PC wires.

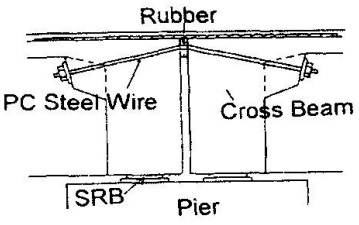

Fig. 4 Girder Connection

2.3 Restrainers

A restrainer which could work in directions both longitudinal and lateral was required for an omnidirectional isolation system. Rubber-sheathed chains as shown in **Fig. 5** were adopted. Their impact-absorbing properties can also minimize the probability of destruction due to impact. An impact-tension test was conducted to check the impact-absorbing capability with a high-speed tension tester.

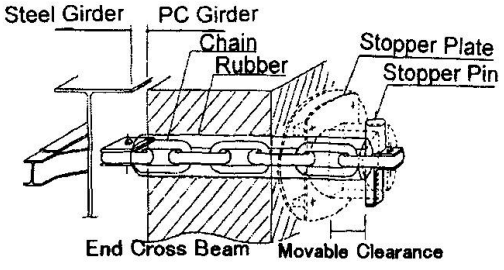

Fig. 5 Restrainer with Rubber-sheathed Chain